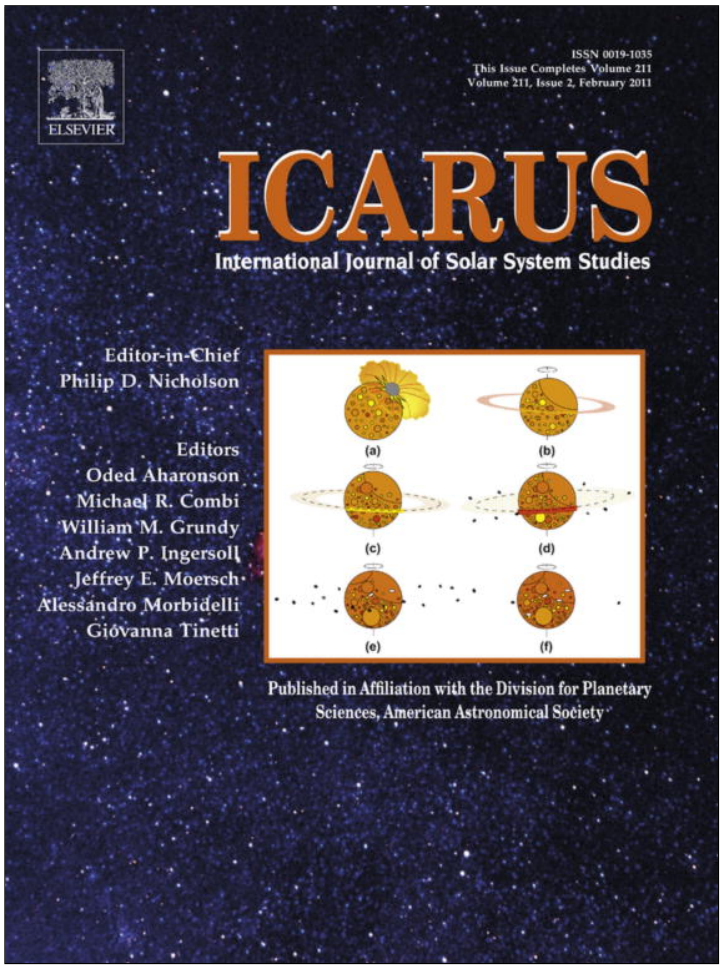

Icarus 211 (2011) 1179–1203

Contents lists available at ScienceDirect

Icarus

journal homepage: www.elsevier.com/locate/icarus

The volcanic history of Mars: High-resolution crater-based studies of the calderas of 20 volcanoes

Stuart J. Robbins [a,*], Gaetano Di Achille [a,1], Brian M. Hynek [a,b]

[a] Laboratory for Atmospheric and Space Physics, University of Colorado at Boulder, UCB 392, Boulder, CO 80309, United States
[b] Department of Geological Sciences, University of Colorado at Boulder, UCB 392, Boulder, CO 80309, United States

ARTICLE INFO

Article history:
Received 11 May 2010
Revised 1 November 2010
Accepted 9 November 2010
Available online 19 November 2010

Keywords:
Mars
Cratering
Mars, Surface
Volcanism

ABSTRACT

Determining absolute surface ages for bodies in the Solar System is, at present, only possible for Earth and Moon with radiometric dating for both bodies and biologic proxies such as fossils for Earth. Relative ages through cratering statistics are recognized as one of the most reliable proxies for relative ages, calibrated by lunar geologic mapping and Apollo program sample returns. In this work, we have utilized the Mars Reconnaissance Orbiter's ConTeXt Camera's images which provide the highest resolution wide-scale coverage of Mars to systematically crater-age-date the calderas of 20 of Mars' largest volcanoes in order to constrain the length of time over which these volcanoes – and major volcanic activity on the planet, by extension – were active. This constitutes the largest uniform and comprehensive research on these features to date, eliminating unknown uncertainties by multiple researchers analyzing different volcanoes with varied data and methods. We confirm previous results that Mars has had active volcanism throughout most of its history although it varied spatially and temporally, with the latest large-scale caldera activity ending approximately 150 ma in the Tharsis region. We find a transition from explosive to effusive eruption style occurring in the Hesperian, at approximately 3.5 Ga ago, though different regions of the planet transitioned at different times. Since we were statistically complete in our crater counts to sizes as small as ~60 m in most cases, we also used our results to study the importance of secondary cratering and its effects on crater size–frequency distributions within the small regions of volcanic calderas. We found that there is no "golden rule" for the diameters secondaries become important in crater counts of martian surfaces, with one volcano showing a classic field of secondaries ~2 crater diameters from the center of its primary but not affecting the size–frequency distribution, and another clearly showing an influence but from no obvious primary.

Published by Elsevier Inc.

1. Introduction

The planet Mars has had an active geologic past with a varied surface showing evidence of past fluvial, aeolian, and volcanic activity. This is in stark contrast with the current lack of geologic activity on Mars, though recent data have illustrated a few lingering aeolian and cryogenic processes that continue to significantly shape its surface (*e.g.*, Hartmann, 2005). Noticeably missing from the list of current activity is volcanism, and an ongoing question has been when the last volcanic episodes occurred on Mars.

Many researchers in the past have tried to answer when volcanism ended through two methods. The method that we will not be addressing in this paper involves radiometric dating of the known martian meteorites, which generally date from a few hundred Ma to about 1.5 Ga, the noticeable exception being ALH84001 which dates to ~4.5 Ga (Nyquist et al., 2001) though recent estimates place it at ~4.1 Ga (Lapen et al., 2010). The basaltic meteorites (ALH84001 is an orthopyroxenite) require volcanism at the time of formation, constraining the most recent episode on Mars to a maximum of 180 myr ago (the basaltic shorgottite meteorites Shergotty, Zagami, and Los Angeles) (Bouvier et al., 2005).

The second method of age dating the martian volcanoes is crater-based, an established technique that assumes an older surface will have a higher crater density because it has had more time to accumulate craters (Arvidson et al., 1979). Since the original images from the Mariner 9 and Viking orbiters were returned in the late 1960s and throughout the 1970s, different researchers have tried to use crater densities to successively refine the ages of the major volcanoes on the planet (*e.g.*, Blasius, 1976; Plescia and Saunders, 1979; Neukum et al., 1979; Neukum and Hiller, 1981; Greeley and Spudis, 1981; Plescia, 1994; Hodges and Moore, 1994 and references therein). In general, the utility of crater counting is greatly increased when (a) larger areas are used and (b) smaller craters are included for the joint effect of better number

* Corresponding author. Fax: +1 303 492 6946.
E-mail addresses: stuart.robbins@colorado.edu (S.J. Robbins), Gaetano.DiAchille@lasp.colorado.edu (G.D. Achille), hynek@lasp.colorado.edu (B.M. Hynek).
[1] Present address: Research and Scientific Support Department, ESA-ESTEC, NL, Noordwijk, The Netherlands.

0019-1035/$ - see front matter Published by Elsevier Inc.
doi:10.1016/j.icarus.2010.11.012

statistics and a larger range of diameters for age determinations. The latter is limited usually by the data resolution for airless or nearly-airless bodies, such as Mars or the Moon.

The last 15 years has brought more orbiters to Mars with ever-higher-resolution cameras, allowing crater-based age dating of the volcanoes to be refined by dating individual features such as flows, collapses, and calderas (*e.g.*, Hartmann, 2005). It has only been in the last ~6 years that the planetary community has had sufficient imagery to derive statistically meaningful ages from areas that are as small as volcanic calderas on the planet, mainly through the use of Mars Express' High Resolution Stereo Camera (HRSC, roughly 10–30 m/pix resolution) and Mars Reconnaissance Orbiter's (MRO's) ConTeXt Camera (CTX, 5.5–7.5 m/pix resolution), resulting in works such as Neukum et al. (2004), Werner (2009), and this work. Previous work with Mars Global Surveyor's Mars Orbiter Camera (MOC) by different researchers in localized parts of the planet that illustrates some lava flows are as young as a few 10s of millions of years (*e.g.*, Berman and Hartmann, 2002; Hartmann, 2005; Roberts et al., 2007).

Neukum et al. (2004) used HRSC images to age-date five volcanic summits – Hecates and Albor Tholi located in Elysium, and Arsia, Ascraeus, and Olympus Montes located in the vast Tharsis region (Fig. 1). Their work is comparable to ours except in number of volcanoes dated and our completeness to decameter-scale craters. Since then, the only researcher to attempt to systematically crater-age-date the volcanic calderas was Werner (2009) who dated all 24 major volcanic constructs using HRSC data, but often all calderas were combined into one, or the calderas were not dated in favor of analyzing the flanks or other flows from the volcanoes.

Our aim was to use the CTX dataset, which offers up to 6× higher resolution than HRSC, to systematically crater-age-date recognizable calderas in the 24 major volcanoes on Mars (Fig. 1). The previous work to systematically date the volcanoes (Werner, 2009) used HRSC, while all previous research was done by different people using various datasets, lacking much consistency when looking at absolute ages at the 10–100 myr precision level. This limits their utility in providing a timeline for volcanism on the planet. In this work, we were able to date 93 calderas within 20 volcanoes using a uniform, high-resolution dataset, and all the crater counting was done by a single person; the four volcanoes southeast of the Hellas impact basin (Amphitrites, Malea, Peneus, and Pityusa Paterae) have inadequate CTX coverage for this approach as of May 2010 and were not analyzed. We use these data to (a) confirm previous results of continuous volcanism throughout Mars' history until the recent past, (b) argue for dwindling and increasingly localized volcanism through time, (c) discuss the implications of the ages for the eruptive history of the Tharsis region, (d) provide a transition time from explosive to effusive volcanism, and (e) explore ancillary issues of secondary cratering and resurfacing rates.

We discuss our methods of mapping the main volcanic calderas on Mars and crater-age dating in Section 2. Sections 3–7 are devoted to our analysis and results for each volcano with each section describing a different province: Tharsis (Section 3), Syrtis Major (Section 4) and Elysium (Section 5) regions, Apollinaris Mons (Section 6), and the volcanoes surrounding Hellas Basin (Section 7). We then use these results to discuss implications for secondary cratering and resurfacing in Section 8, and finally the implications for the most recent volcanism in various regions of the planet in Section 9. We list the areas of calderas and number of craters identified in Table 1, and we summarize our age results in Table 2.

2. Method

2.1. Image processing

We obtained the highest resolution visible images available with the widest coverage from a single source, the CTX dataset (Malin et al., 2007) from the MRO spacecraft. This instrument records greyscale images of the martian surface at resolutions in the range ~5.5–7.5 meters per pixel (m/pix) that are publicly available through NASA's online Planetary Data Systems (PDS) website (http://www.pds-imaging.jpl.nasa.gov/). We obtained the best images in terms of data quality and with the most complete coverage available for our study areas as of May 2010.

The images were processed using the United States Geological Survey's (USGS's) Integrated Software for Imagers and Spectrometers (ISIS) v 3.1 software. They were mosaicked together, projected to a standard equicylindrical spheroid, and output at a final, uniform resolution that was slightly down-sampled from the original to 10 m/pix. This was done to limit the final file sizes to a few

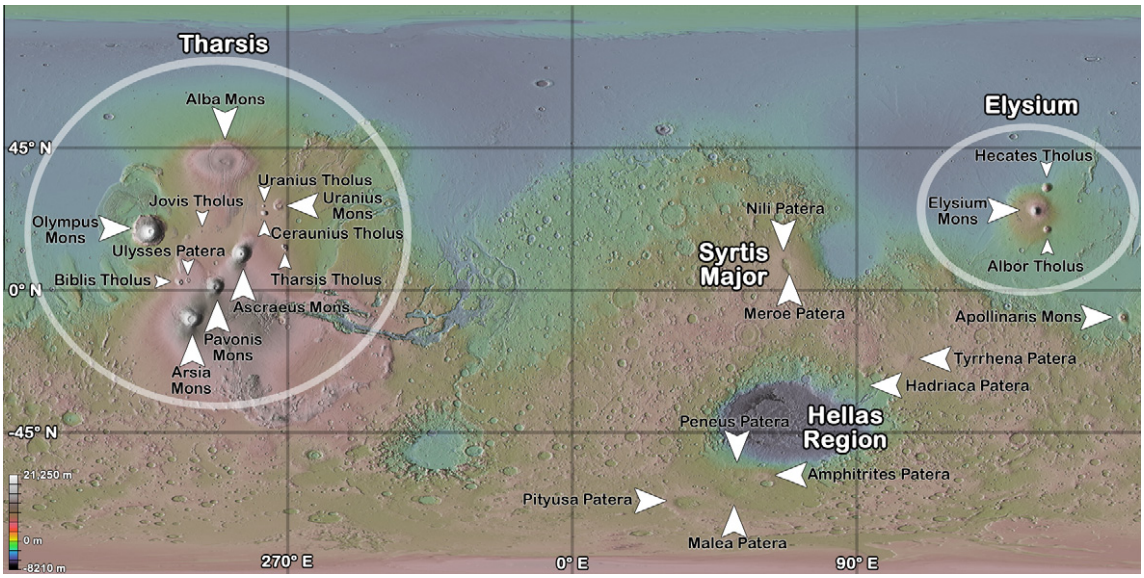

Fig. 1. Underlying map is MOLA (Mars Orbiter Laser Altimeter) shaded relief (Smith et al., 2001), with the arrows and labels showing the locations of the two dozen major identified volcanoes on the planet. Arrow orientation and size is not coded to anything. All volcanoes except those southeast of Hellas Basin were analyzed.

Table 1
Area of calderas and number of identified craters of all volcanoes (first line km^2, second line number of craters counted) – total area: 51,545 km^2.

Volcano	1	2	3	4	5	6	7	8	9	Total
Alba	2210[a] 3140	354[b] 170	10.8[b] 29	51.4[b] 79	7010[b] 3534	325[b] 438				9966 7390
Albor	35.5[b] 221	104[b] 154	237[b] 100	55.3[b] 505						432 980
Apollinaris	1530[b] 6293	1420[b] 4455	583[a] 755	93.2[a] 388	164[a] 582	109[a] 370				3898 12,843
Arsia	9840[b] 39,674									9837 39,674
Ascraeus	508[b] 1683	107[b] 706	274[b] 3177	196[b] 1526	74.2[b] 203	8.02[b] 25	35.7[b] 307			1203 7627
Biblis	65.9[b] 13	528[b] 232	449[b] 242	58.2[b] 22						1101 509
Ceraunius	237[b] 1279	39.6[b] 217	13.9[a] 118	18.8[a] 181						310 1795
Elysium	10.4[a] 301	144[a] 2985	12.0[a] 212							167 3498
Hadriaca	1600[a] 4721	88.1[a] 388	433[a] 1424	195[a] 659	224[a] 451	80.5[a] 160	360[a] 1576	154[a] 391	738[a] 2009	3874 11,779
Hecates	10.9[b] 6	14.8[b] 24	12.1[b] 23	10.3[b] 34	18.3[b] 58					66.4 145
Jovis	423[b] 791	6.34[b] 17	1.12[b] 6	27.7[b] 41	28.8[b] 54	11.6[a] 23	123[a] 234			621 1166
Meroe	539[b] 756	443[b] 634	361[b] 472	275[b] 547	27.7[b] 17	165[b] 214	14.4[b] 27	10.9[b] 23		1836 2690
Nili	121[b] 202	204[b] 303	138[b] 374	939[b] 1889	47.7[b] 61					1452 2829
Olympus	218[b] 1307	238[b] 920	945[b] 3963	240[b] 1240	1590[b] 8115	77.3[b] 246				3308 15,791
Pavonis	678[b] 951	0.612[b]	10.3[b]	4200[b] 7314						4335 8265
Tharsis	312[b] 463	148[b] 331	9.29[b] 13	14.8[b] 35	101[b] 117	224[a] 161	14.4[b] 23			884 1143
Tyrrhena	389[a] 2028	44.6[a] 177								434 2205
Ulysses	701[b] 737									701 737
Uranius M.[*]	1680[b] 7058	857[b] 2740	130[b] 323	136[b] 329	339[b] 519	24.9[b] 155	16.1[b] 24			3183[*] 11,148
Uranius T.	88.4[b] 204	261[a] 706								349 910

[*] Due to poor CTX data, only ~50% of Uranius Mons was analyzable. Actual areas for the calderas are: 3410, 1340, 486, 136, 755, 88.4, and 52.4 km^2, for a total area of 6259 km^2.
[a] Denotes a caldera with volcanism that was primarily explosive/pyroclastic.
[b] Denotes a caldera with volcanism that was primarily effusive.

hundred MB to make it easier to work with on modern workstations while still having enough resolution to accurately identify $D \geqslant 50$ m craters. The mosaics for each volcano were then imported to ESRI's ArcGIS software and the projection was confirmed by using the THEMIS Daytime IR global mosaics (Christensen et al., 2004) as a base map.

2.2. Geomorphologic mapping

Geomorphologic mapping was performed for all the studied volcanic summits. Map units were digitally drafted in a GIS environment using standard photogeologic techniques (*i.e.*, Tanaka et al., 2005; Hare et al., 2009). The geomorphologic-based interpretation of the volcanic features mainly relied on the CTX image mosaic base map and MOLA gridded topography (463 m/pix at equator). High resolution images (*e.g.* MOC, HiRISE, etc.) and topography (*e.g.* HRSC DEMs) were consulted in the cases of ambiguous contacts at CTX and MOLA scales, respectively. A combination of different criteria, including textural, morphological, topographic, and thermophysical properties (Putzig and Mellon, 2007), were used to differentiate the map units. Particularly, (a) textural/albedo pattern changes (*e.g.* smooth vs. rugged, or dark vs. bright surfaces), (b) morphologies such as scarps, terraces, and wrinkle ridges, and (c) topographic structures like circular collapsed areas and/or raised blocks throughout the main calderas of the volcanic complexes were used to distinguish several possible nested calderas.

We used a liberal approach discriminating as many subunits as possible. On one hand, this is against the general indications regarding mapping volcanic units on Mars. In fact, Tanaka et al. (2009) suggested that division of volcanic units on Mars is justified only for the clearest cases of distinctive primary characteristics. On the other hand, our speculative approach is aimed at providing a detailed reconstruction of the sequence of volcanic events within

Table 2
Modeled crater ages for each caldera with diameter range (first line, meters) and derived age (second line). Question marks indicate an ambiguous and suspect age.

Volcano	1	2	3	4	5	6	7	8	9
Alba	600–1000 $3.02^{+0.32}_{-0.91}$ Ga	~800/147–180 >2.0 G/210 ± 50 M	–	110–150 580 ± 110 Ma	500–930 2.03 ± 0.42 G	160–250 450 ± 100 Ma			
Albor	113–282 1.50 ± 0.36 Ga	175–247 940 ± 270 Ma	126–408 1.01 ± 0.31 Ga	382–474 $3.53^{+0.07}_{-0.13}$ Ga					
Apollinaris	342–641 $3.57^{+0.03}_{-0.04}$ Ga	373–699 $3.52^{+0.05}_{-0.07}$ Ga	95–118/1079–1525 $200 \pm 20M/3.93^{+0.06}_{-0.10}$ Ga		390–814 $3.77^{+0.04}_{-0.06}$ Ga	66–97/416–551 $220 \pm 30M/3.54^{+0.11}_{-0.52}$ G			
Arsia	144–615 130 ± 20 Ma								
Ascraeus	60–167 250 ± 20 Ma	58–157 320 ± 50 Ma	67–129 1.06 ± 0.05 Ga	66–167 730 ± 60 Ma	80–93/124–187 230 ± 30/320 ± 100 M		53–86/116–126 570 ± 60/230 ± 90 Ma		
Biblis	222 <480 ± 270 Ma	350–539 $3.20^{+0.19}_{-0.67}$ Ga	288–357 2.10 ± 0.44 Ga	357–381 $3.35^{+0.19}_{-1.45}$ Ga					
Ceraunius	89–121/160–247 470 ± 40/630 ± 140 Ma	74–109 400 ± 70 Ma	55–69/157–288 $510 \pm 70M/3.41^{+0.13}_{-0.62}$ Ga	50–58/179–227 $590 \pm 50M/3.59^{+0.05}_{-0.08}$ Ga					
Elysium	102–171 $3.11^{+0.21}_{-0.57}$ Ga	87–237 $2.77^{+0.20}_{-0.23}$ Ga	106–208 $3.17^{+0.19}_{-0.58}$ Ga						
Hadriaca	551–888 $3.55^{+0.06}_{-0.11}$ Ga	253–398 $3.27^{+0.19}_{-0.98}$ Ga	258–576 1.79 ± 0.45 Ga	– –	227–373 1.62 ± 0.46 G	641–814 $3.57^{+0.10}_{-0.37}$Ga	– –	288–314/425–576 $2.11^{+0.66}_{-0.67}/3.55^{+0.10}_{-0.33}$Ga	407–551 $3.25^{+0.16}_{-0.57}$Ga
Hecates	93–104 200 ± 110 M?	70–106 220 ± 80 M?	135–157 1.01 ± 0.46 G?	217–270 $3.52^{+0.11}_{-0.57}$ G?	187–212 $2.67^{+0.59}_{-1.00}$ G?				
Jovis	232–357 2.16 ± 0.38 Ga	89–116 840 ± 300 Ma	102–113/321–342 440 ± 110 M/>2 G?	– –	104–144 400 ± 140 M	187–232 $2.78^{+0.58}_{-1.42}$ Ga	183–321 1.76 ± 0.44 Ga		
Meroe	373–528 $2.95^{+0.35}_{-0.80}$ Ga	270–563 $2.95^{+0.29}_{-0.55}$ Ga	276–474 $3.03^{+0.27}_{-0.66}$ Ga	– –	106–116/213–242 230 ± 90 M/>1.4 G	328–416/463–684 $3.63^{+0.04}_{-0.06}/3.77^{+0.05}_{-0.08}$ Ga		141–154 $2.05^{+0.66}_{-0.67}$ Ga	
Nili	212–264/365–516 $3.02^{+0.24}_{-0.51}/3.55^{+0.09}_{-0.22}$ Ga	247–335 1.61 ± 0.50 Ga	237–381 2.04 ± 0.25 Ga	– –	– –				
Olympus	57–113/141–217 380 ± 20/240 ± 70 Ma	97–113/144–217 360 ± 30/140 ± 50 Ma	62–104/164–253 330 ± 10/240 ± 40 Ma	67–116/150–227 420 ± 30/260 ± 70 Ma	57–91/154–321 340 ± 10/250 ± 40 M	45–111 140 ± 20 Ma			
Pavonis	83–119 130 ± 20 Ma	– –	– –	300–601 860 ± 170 Ma					
Tharsis	321–463 $2.46^{+0.63}_{-0.75}$ Ga	288–350 $3.24^{+0.17}_{-0.62}$ Ga	191–247 1.73 ± 0.80 Ga	– –	258–294 $2.64^{+0.54}_{-0.78}$ G	357–425 $3.02^{+0.34}_{-1.00}$ Ga	179–195 1.34 ± 0.72 Ga		
Tyrrhena	282–528 $3.41^{+0.08}_{-0.16}$ Ga	– –							
Ulysses	264–407 1.42 ± 0.30 Ga								
Uranius M.	227–551 $3.19^{+0.10}_{-0.19}$ Ga	237–516 $3.43^{+0.05}_{-0.07}$ Ga	191–217 780 ± 20 Ma	258–365 $2.90^{+0.39}_{-0.82}$ Ga	300–474 $3.25^{+0.15}_{-0.50}$ G	141–195 $3.34^{+0.10}_{-0.22}$ Ga	46–60/116–132 80 ± 20/430 ± 180 Ma		
Uranius T.	264–381 $3.57^{+0.06}_{-0.09}$ Ga	390–454 $3.56^{+0.06}_{-0.10}$ Ga							

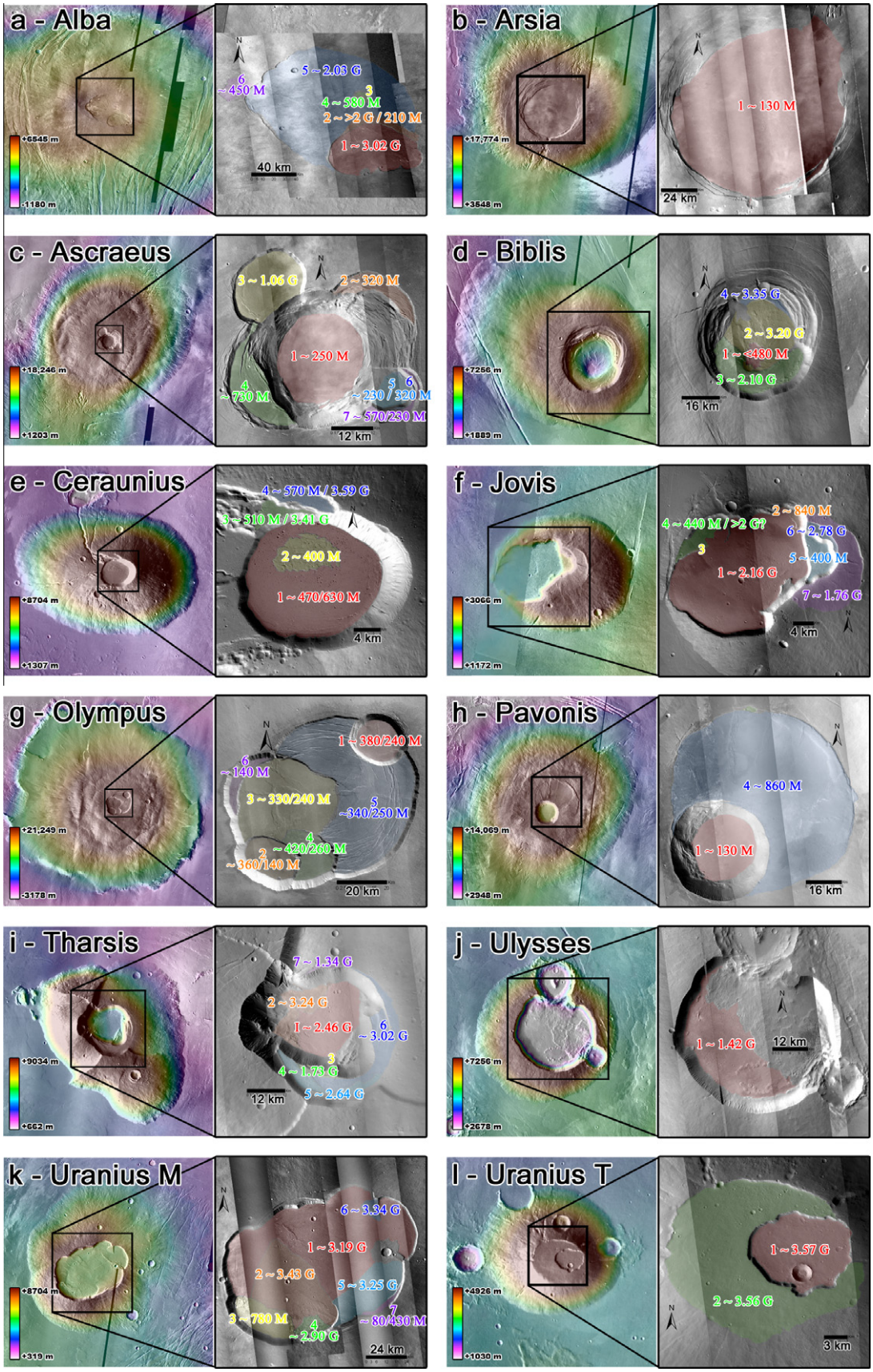

Fig. 2. Left panels from each pair shows MOLA altimetry color-coded map with THermal EMission Imaging Spectrometer (THEMIS) Daytime IR underlaid for context, showing the entire volcano that we studied. Colored and labeled regions correspond to the different calderas that we identified on each summit. Call-out boxes indicate ages that we calculated, but due to readability, uncertainties are only included in the text. Volcanoes in this figure are Alba Mons (a), Arsia Mons (b), Ascraeus Mons (c), Biblis Tholus (d), Ceraunius Tholus (e), Jovis Tholus (f), Olympus Mons (g), Pavonis Mons (h), Tharsis Tholus (i), Ulysses Patera (j), Uranius Mons (k), and Uranius Tholus (l). These are the twelve Tharsis province volcanoes that we studied in Section 3.

each of the studied volcanic complexes. Nevertheless, although some of the several possible subcalderas were identified and discriminated based on subtle criteria, the majority of them were mapped based on conservative and characteristic temporal evidence such as stratigraphic superposition relationships, and tectonic, topographic structures, and/or erosional features suggesting modification of one specific unit but not the adjacent terrain. We show our caldera delineation in Figs. 2 and 3.

Moreover, while we performed separate crater counts for each caldera mapped, we considered these speculative and a few were later combined for the final analysis discussed in Sections 3–7. There were occasional issues with mapping and our original goal of mapping each individual caldera event was offset by a more pragmatic approach of mapping each possible eruption event; the most obvious cases were Alba Mons (Section 3.1, Fig. 2a) and Uranius Mons (Section 3.11, Fig. 2k). Finally, all the surficial materials clearly superposed on the studied calderas as a result of relatively young resurfacing events were excluded from the final mapped units and thus not considered during the crater counting. These include any inferred glacial deposits and rock glaciers, alluvial materials, aeolian features, landslides, and significant crater ejecta blankets superimposed on the caldera units.

The schema in caldera numbering within each volcanic summit was based primarily on the caldera with the lowest elevation being numbered "1," second-lowest "2," etc. If it was not obvious at a glance as to what caldera was lower than another, then calderas were numbered subsequently from the closest to caldera 1 and outwards (*e.g.*, the closest would be caldera 2, next caldera 3, etc.). This is apparent in the mapping of Albor Tholus. Otherwise, in cases where elevation was not readily apparent, calderas were numbered in a counter-clockwise direction; this was used for example in the numbering of Ascraeus Mons.

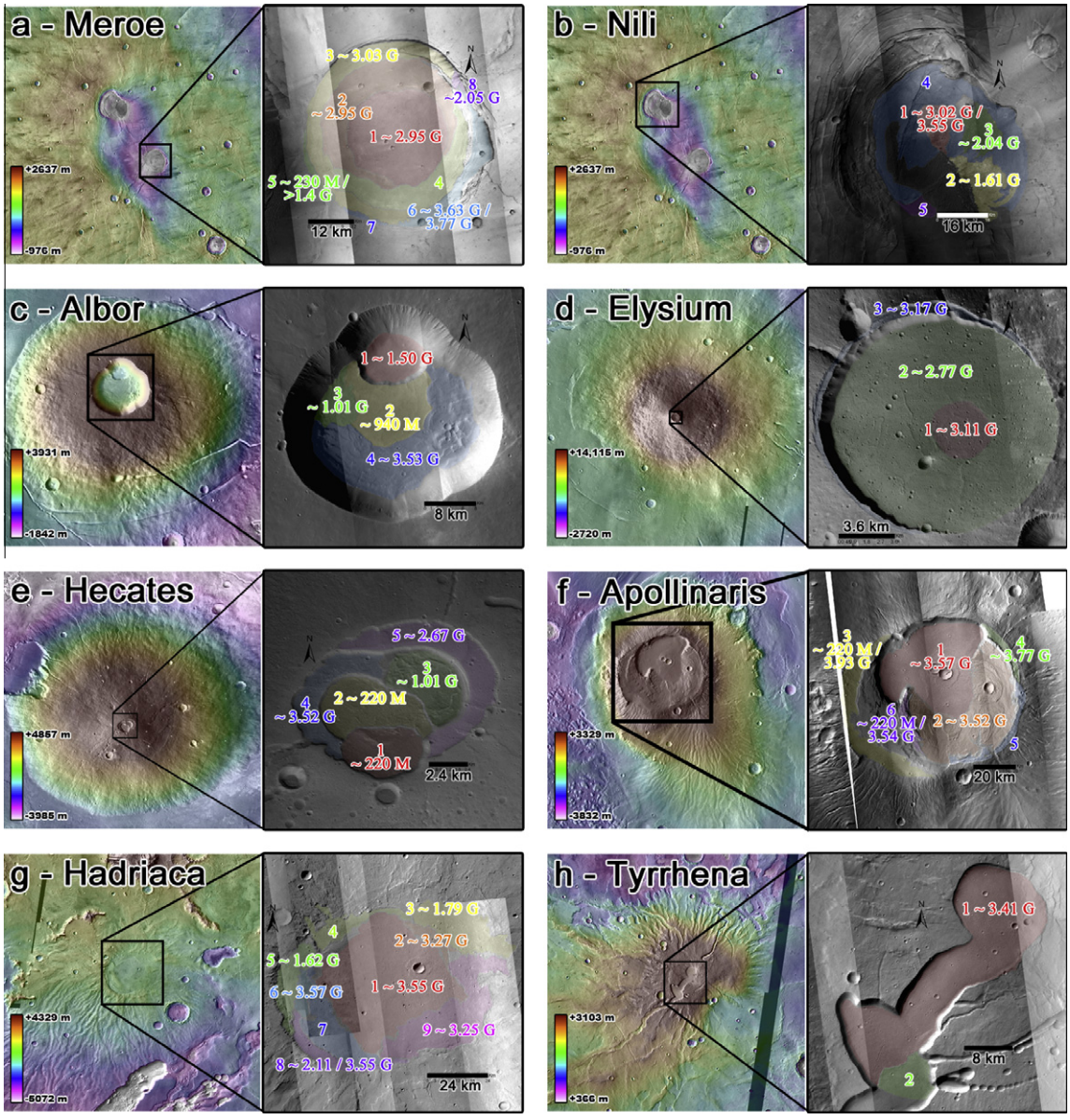

Fig. 3. Left panels from each pair shows MOLA altimetry-color-coded map with THEMIS Daytime IR underlaid for context, showing the entire volcano that we studied. Colored and labeled regions correspond to the different calderas that we identified on each summit. Call-out boxes indicate ages that we calculated, but due to readability, uncertainties are only included in the text. Volcanoes in this figure are Meroe Patera (a), Nili Patera (b), Albor Tholus (c), Elysium Mons (d), Hecates Tholus (e), Apollinaris Mons (f), Hadriaca Patera (g), and Tyrrhena Patera (h). These are the two Syrtis Major calderas (a and b) discussed in Section 3, the three Elysium province volcanoes (c–e) discussed in Section 4, the lone Apollinaris discussed in Section 5, and the two northwest Hellas Basin volcanoes (g and h) discussed in Section 6.

2.3. Crater counting

In ArcGIS, craters were visually identified within each caldera with the base CTX map over-sampled to a scale of 1:10,000 on-screen. Exogenic craters (from extra-planetary impactors) were differentiated from endogenic craters (such as collapse pits) by general standard morphologic characteristics, such as a raised rim and the steepness of the crater walls, while special care was given to craters lying within, on, or near any extensional features or potential collapsed lava tube features. Very tight clusters of craters that displayed near-vertical walls and flat floors were also treated as endogenic due to their probable sublimation-collapse origin and lack of exogenic impact crater characteristics (see Fig. 4). Crater rims were outlined using ArcGIS's Editing Tools by laying down one vertex every 25 m. The combination of oversampling visually (viewing one pixel on the map as more than one pixel on the screen) and undersampling in outlining (creating one vertex for every ~2.5 pixels as opposed to every pixel) helped to reduce errors in outlining rims and reduce the time necessary for this task due to a decreased need for higher precision manual dexterity. Vertexes were recorded in decimal degrees. The polygons representing each crater rim were then imported into Igor Pro software where we used an in-house non-linear least-squares (NLLS) fitting algorithm to a circle to determine the center latitude and longitude of each crater as well as its diameter.

The NLLS algorithm corrects for map projection by converting the decimal degrees into meters from the polygon's centroid, accounting for the 1st-order spherical surface of Mars. Although this is a minor correction for craters on the hectometer scale, nonetheless it would noticeably affect fitted diameters of craters at latitudes larger than ~±30° (*e.g.*, Alba Mons). Similarly, the polygons representing volcanic calderas were imported into Igor Pro and the area was calculated using a standard geometric method after applying the afore-mentioned map projection correction. The areas for each volcanic caldera and the number of craters identified within it are shown in Table 1.

2.4. Size–frequency diagrams and isochron-fitting

After crater rims were analyzed and diameters calculated, standard crater size–frequency diagrams (SFDs) were created (Arvidson et al., 1979) with slight modifications, as detailed in this subsection. These were done by binning data in multiplicative $2^{1/32}D$ intervals. Finer binning than the more standard $2^{1/2}D$ was used to bring out detail in the SFDs that would otherwise be obscured as well as to give the appearance of more continuous data given the number of craters in this study (Table 1). Craters were placed into bins such that $D_{\text{bin-1}} < D_{\text{crater}} \leqslant D_{\text{bin}}$. This is effectively a ceiling function (rounds up) that places all craters in a diameter bin that is the largest crater size in that bin. If the distribution of craters were even across all diameters, then a simple average $\overline{D}_{\text{bin}_a} = (D_{\text{bin}_a} + D_{\text{bin}_{a-1}})/2$ would suffice to place the bin diameters where they should be once binning is completed.

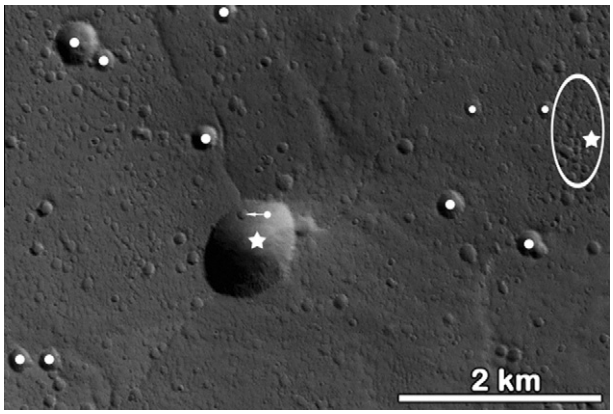

Fig. 4. This is a small region within the Elysium Mons caldera (caldera 2) that illustrates two different types of endogenic craters as well as several exogenic craters. Probable endogenic craters are indicated with a star (the largest crater visible, and the region of craters within the open ellipse). These illustrate the kinds of morphologies more common to endogenic craters discussed in the text. Filled circles indicate some of the larger exogenic craters we identified due to their standard morphologic properties (see text for discussion, Section 2.3).

However, crater SFDs generally follow a $b = -2$ power law. This can be accounted for following Tanaka (1982):

$$\overline{D} = \frac{\int_{D_a}^{D_{a-1}} D dN_c}{\int_{D_a}^{D_{a-1}} dN_c} = \frac{3}{2}\frac{D_a^{-2} - D_{a-1}^{-2}}{D_a^{-3} - D_{a-1}^{-3}} \tag{1}$$

Unfortunately, this correction is still inaccurate because it assumes a fixed slope, and rarely did our SFDs follow that power law (*e.g.*, Figs. 5 and 6). Rather, we factored in the local slope between the bin in question and the next-smallest in order to shift the diameter to a more robust weighted mean; this has a side-effect of having bins that are not evenly spaced in $\log(D)$:

$$D_a = \frac{D_a - D_{a-1}}{1 + N(D_{a-1})/N(D_a)} + D_{a-1} \tag{2}$$

where $N(D_a)$ is the number of craters at diameter bin D_a. While this is a better approximation than Tanaka (1982), it is not a substitute for ever-finer binning resolution.

With the incremental SFD created, we coded an additional three options into our SFD algorithm. The first removes the largest bins with too few craters – we set this cut-off at less than three craters in a cumulative bin to eliminate some issues with small-number statistics. The second option removes incremental bins that had no craters within them, effectively no new information. That is why there is a lack of data at some diameter locations in many of our SFDs (Figs. 5 and 6). The final option removes diameter bins smaller than our statistical completeness. For this purpose, we defined statistical completeness as the incremental bin with the greatest number of craters. Error bars were calculated by standard $\sqrt{N}$ Poisson statistics (Arvidson et al., 1979).

Once these operations were performed, the incremental SFDs were integrated to yield a cumulative SFD. All SFDs in this paper are cumulative. SFDs were then scaled by the caldera area, and we show them for the volcanoes we studied in Figs. 5 and 6 (higher resolution versions of each panel in Figs. 5 and 6 are available in online supplemental material).

Isochrons are based on the method of Ivanov (2001) and Neukum et al. (2001). A 1 Ga isochron is created from an 11th-order polynomial production function for Mars, based on lunar crater counts and absolute ages. Another function calculates how the 1-km point should be scaled based upon the impact flux through time based on scaling from Apollo sample return calibration of the lunar isochrons. Isochron shape does not change based on age, only the crater density (vertical offset in our plots).

To fit our data to an isochron, we used a range of diameters rather than relying upon a perhaps more standard $N(1)$ age. $N(1)$ ages proved insufficient for our study due to (a) the calderas rarely having craters as large as 1 km, and (b) the SFDs rarely falling on the same isochron at 1 km as at 100 m. We selected diameter ranges that paralleled the isochron function; other diameter ranges that did not were assumed to be affected by weathering (erosion, infilling, etc.), incomplete counts (for $D < 50$–70 m), contamination by secondaries, or other non-age-related issues. Since our objective was to determine ages, we simply needed to find a range of diameters that fit the established isochrons. We created an algorithm to calculate the average difference between the SFD points and the model 1 Ga isochron, weighting each point the same. Using the

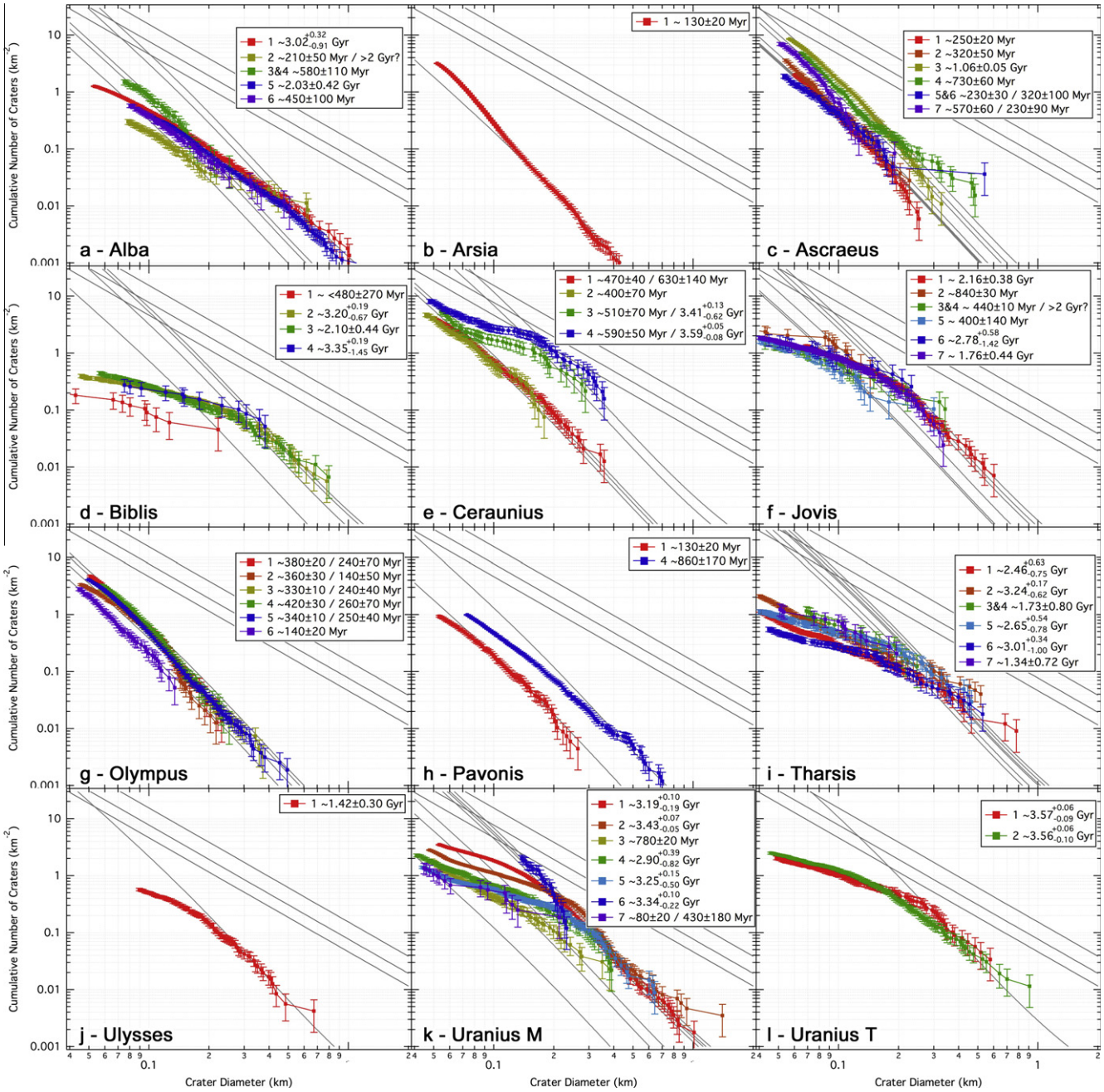

Fig. 5. Size–frequency distributions for the Tharsis volcanoes in the same order as Fig. 2: Alba Mons (a), Arsia Mons (b), Ascraeus Mons (c), Biblis Tholus (d), Ceraunius Tholus (e), Jovis Tholus (f), Olympus Mons (g), Pavonis Mons (h), Tharsis Tholus (i), Ulysses Patera (j), Uranius Mons (k), and Uranius Tholus (l). Colors on SFDs correspond to the colors used in the Fig. 2 for each volcano such that, for example, the red curve corresponds to caldera 1 in all cases. Steep diagonal grey lines are the isochrons for ages found in the legends of each panel. Shallow diagonal grey lines represent 10%, 5%, and 3% of geometric saturation based on the standard $1.54D^2$ value for geometric saturation (Melosh, 1989). Larger versions of each volcano's caldera SFD are available in supplementary material online.

time scaling function discussed above, we then determined the age that best fit our selected diameter range.

We determined uncertainties in our ages by taking our formal $\sqrt{N}$ error bars at each diameter bin used in the fitting and first adding them to the SFD data point. We then calculated the best-fit isochron for the new SFD. Third, we subtracted the error from the original SFD points and calculated the best-fit isochron. The original model isochron age was then subtracted from these new fitted ages to estimate the plus/minus uncertainties in each determined age. Due to the nature of the time scaling function, ages younger than ~2.5 Gyr have symmetric uncertainties. Older ones generally have larger negative uncertainties than positive.

In addition to isochrons on our SFD plots, we show 10%, 5%, and 3% lines of geometric saturation, where geometric saturation is defined by a surface having enough craters such that the creation of a new one will eliminate an equivalent existing one (Melosh, 1989). The equation for geometric saturation, $1.54D^{-2}$, has a shallower slope than isochrons and hence saturation occurs for younger ages at smaller crater sizes. One hundred percent geometric saturation does not exist on real planetary surfaces, and they generally saturate at only a few percent of geometric values. Consequently, we

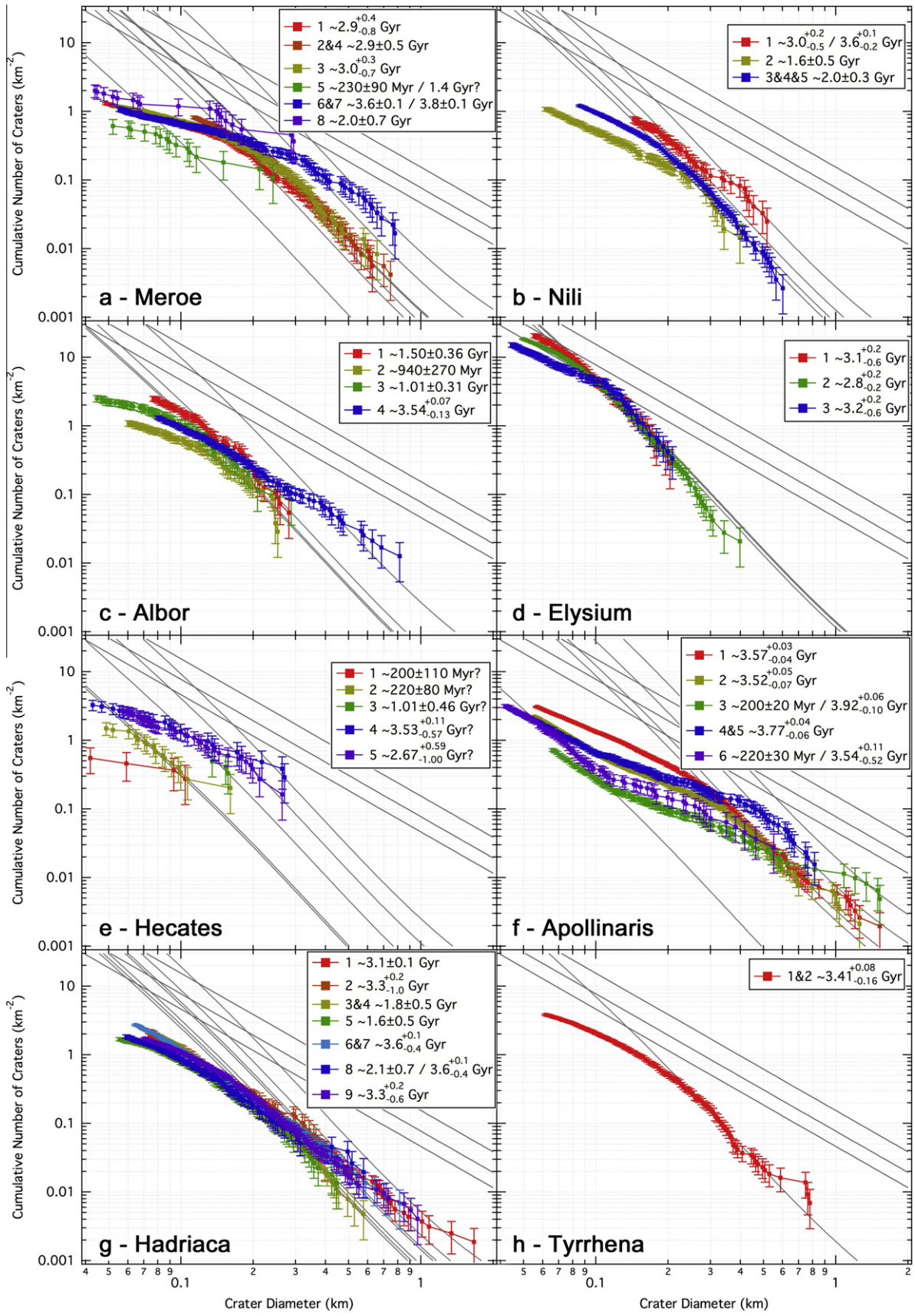

Fig. 6. Size–frequency distributions for the non-Tharsis volcanoes in the same order as Fig. 3: Meroe Patera (a), Nili Patera (b), Albor Tholus (c), Elysium Mons (d), Hecates Tholus (e), Apollinaris Mons (f), Hadriaca Patera (g), and Tyrrhena Patera (h). Colors on SFDs correspond to the colors used in Fig. 3 for each volcano such that, for example, the red curve corresponds to caldera 1 in all cases. Steep diagonal grey lines are the isochrons for ages found in the legends of each panel. Shallow diagonal grey lines represent 10%, 5%, and 3% of geometric saturation based on the standard $1.54D^2$ value for geometric saturation (Melosh, 1989). Larger versions of each volcano's caldera SFD are available in supplementary material online.

show various fractions since a surface may be empirically saturated at some smaller fraction of geometric saturation; in our work, we found some cases of saturation in the range 1–4% of geometric.

We note that the martian isochrons are constrained by correlating lunar crater ages with Apollo sample return absolute ages and then extrapolating to Mars based on its surface gravity, proximity to the asteroid belt, impactor velocities at ~1.4 AU, and other scaling differences (Ivanov, 2001), but there is no absolute age dating that can yet be done for martian samples from a known location and geologic unit. Consequently, estimates of crater model ages for Mars are estimated at present to be within a factor of ~2 (Neukum et al., 2004; Hartmann, 2005). While we quote ages in this paper to the 10 Myr and our main literature comparison (Werner, 2009) quotes ages to the 1 Myr level, we realize that the inherent uncertainties in the isochrons are larger than this in every case. However, assuming similar geologic and environmental environments, the relative chronologies from the crater densities are still accurate, and we would fully expect that when absolute measurements can be done, a surface that we date to 150 Ma will be older than one dated to 100 Ma by approximately a factor of 50%. Hence, rounding to the 100 Myr decimal would be counter-productive given the number of craters studied for this work (Table 1) and for the sake of comparison with other published literature.

3. Tharsis region

The Tharsis region of Mars is the largest topographic feature on the planet. It is a vast volcanic province that covers roughly 25% of the planet's surface. Its margin is roughly circular, with an approximate diameter of 3500 km. The origin of the uplift is considered to be volcanic (*e.g.*, Solomon et al., 2005), though the magmatic source and Tharsis' original location has been debated (Zhong, 2009). Twelve large volcanic constructs cover Tharsis, with five major volcanoes (Alba Mons, Olympus Mons, Ascraeus Mons, Pavonis Mons, and Arsia Mons), and seven smaller ones (Ceraunius Tholus, Uranius Mons, Uranius Tholus, Tharsis Tholus, Jovis Tholus, Biblis Tholus, and Ulysses Tholus). Most of these show an effusive type of volcanism, though notably Alba Mons and Uranius Tholus show evidence of explosive styles; we discuss this further in Section 9. We have analyzed all of these volcanoes through the method described in Section 2. Our modeled crater-count ages are presented below, alphabetically, for these 12 volcanoes. The volcanoes are shown in Fig. 2 and their isochrons in Fig. 5 (higher resolution individual panels of Fig. 5 are available in online supplemental material).

3.1. Alba Mons

Alba Mons is a giant shield volcano that covers the largest area by a single volcano on the planet, its footprint approximated as an ellipse roughly 1500 by 1000 km. The center is located at 40°N, 250°E, and it is the northernmost large volcano on the planet. Its volume is difficult to measure due to its large area and estimates in subtracting out a basal layer, but previous researchers have estimated it at $\sim 2.5 \times 10^6$ km^3 (Ivanov and Head, 2006), making it the largest volcano on Mars by volume (Olympus Mons is roughly $\sim 1.7 \times 10^6$ km^3 in contrast). Alba's summit has one of the most complicated caldera complexes on the planet. After Cattermole and Reid (1984), we identified well over a dozen potential calderas, but we only mapped six separate ones on the summit (Fig. 2a) that represent uniformly-aged surfaces, illustrating our more pragmatic approach. In our final analysis, we combined calderas 3 and 4 due to their small sizes, similar crater ages, and because they are topographically similar. The omission of parts of caldera 5 due to the presence of a probable rock glacier along its southwest walls further illustrates the special considerations we took in our mapping.

Our modeled crater ages of the final calderas are open to some interpretation due to the SFDs failing to parallel isochrons over a large diameter range (Fig. 5a). For example, caldera 1 parallels the 3.0 Ga isochron between 0.6 and 1.0 km, and it trails to lower ages at smaller diameters; this is assumed to be evidence of resurfacing here and in many of the calderas that we studied. Caldera 5 has a few large craters emplaced within it, and fitting between 500 and 930 m yields a modeled crater age of 2.0 Ga. Caldera 6 has a SFD starting at 2.0 Ga but quickly crossing 1.5 Gyr of isochrons to lie on the 450 Ma isochron between 250 and 160 m before it trails off at smaller diameters. For more detailed information, refer to Table 2. With the inherent uncertainties in the crater statistics, calderas 3/4 and 6 have statistically-identical ages, and calderas 1 and 5 are statistically identical. Caldera 2's modeled crater age is statistically unique among Alba's calderas, at least for the main isochron fit, and we conclude that it is the youngest surface on the summit.

3.2. Arsia Mons

Arsia Mons is centered at −8.5°N 239°E and is the southernmost of the three Tharsis Montes which also include Pavonis and Ascraeus Mons. Arsia rises ~12 km above the surrounding surface and 17.5 km above the martian datum. It has an average diameter of 300–400 km and possesses the largest single caldera of any volcano on Mars with a diameter ~90–110 km and an area just under 10,000 km^2 (Table 1). Geomorphologic mapping of the Arsia caldera was straightforward. The only region of uncertainty was toward the northeast where the youngest lava overflowed and continued beyond the crater rim. The extent of this northeastern buried margin was defined by extrapolation of the caldera's circular planform, as shown in Fig. 2b. Only regions within this inferred margin were included in the subsequent counts.

Arsia is not only the largest but also one of the youngest calderas that we were able to age-date. Using a crater diameter range of 144–615 m, we date the caldera to 130 ± 20 Ma (Fig. 5b). This is statistically consistent with previous works by Neukum et al. (2004) and Werner (2009) who calculate 130 and 128 Ma, respectively, with approximately ±20% (~±26 Myr) uncertainty.

An additional feature within the large Arsia caldera is the presence of secondary crater fields. While most secondaries with classic morphology are within a few crater diameters of a large primary, no primary large enough exists in the vicinity of Arsia's caldera. These fields of secondaries (an example is shown in Fig. 7) are plentiful and act to increase the slope on our SFD for craters smaller than ~130 m. The SFD does parallel the 280 Ma isochron between ~55 and 70 m, but we interpret this decreased density as the result of incompleteness in our counts rather than a second age for the surface. In this case, Arsia appears to be a case study for large and numerous fields of secondary craters without an obvious nearby primary to form them, as found previously on Europa by Bierhaus et al. (2005) and Mars by McEwen et al. (2005), and summarized by McEwen and Bierhaus (2006). However, we find the onset of secondaries becoming important around 130 m in this case, as indicated by the increasing slope in the SFD from the established isochron. This is far smaller than the ~1 km onset that McEwen and Bierhaus (2006) predicted, and we discuss this further in Section 8.

An interesting feature of the Arsia summit caldera is the presence of numerous smaller shield volcanoes and vents that postdate the last main event. These small shields are visible from CTX imagery and MOLA topography and have been recently reported throughout the eastern half of Tharsis by Hauber et al. (2009 and references therein). Some dated to approximately 50–100 Ma (Hauber et al., 2010). We also dated one of the vents located at

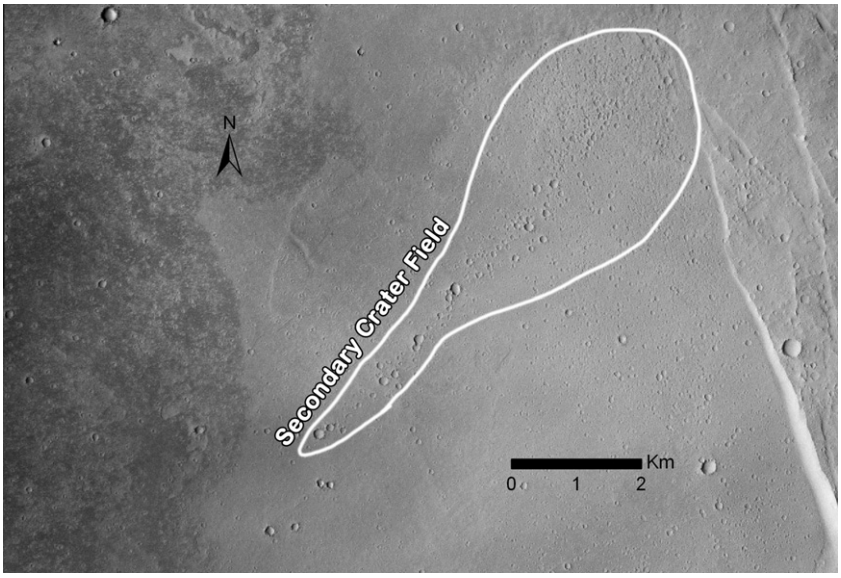

Fig. 7. CTX mosaic image of a small section of Arsia Mons' caldera floor. This shows one of the regions containing fields of obvious secondary craters, centered at −119.55°E, −8.77°W, near the eastern edge of the caldera.

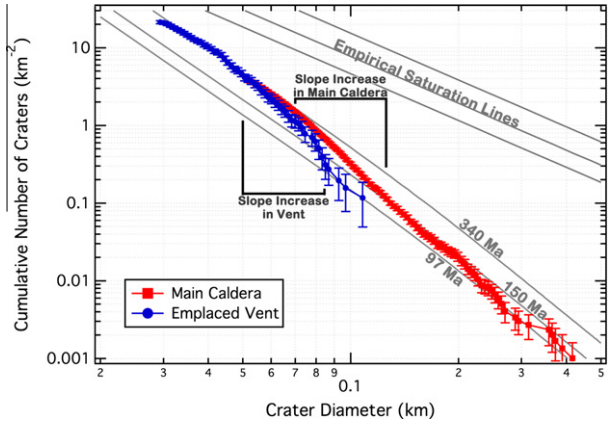

Fig. 8. Size–frequency diagram illustrating the main caldera of Arsia Mons and the youthful vent that we also dated. The "lower" ages for the two are statistically significant, and we attribute the increase in crater frequency at smaller diameters to be a consequence of secondary cratering (*e.g.*, as illustrated in Fig. 7) despite them resting on a 350 Ma isochron.

9.70°S 239.18°E using craters visible in High-Resolution Imaging Science Experiment (HiRISE aboard MRO (McEwen et al., 2007)) image PSP_009343_1700_RED within the Arsia caldera. Our model crater age for this vent is 97 ± 49 Ma – younger than the overall caldera (Fig. 8). The reason for the large uncertainties is that we used the largest three size bins – 93–108 m, which had large statistical uncertainties due to relatively few craters – to date the vent's flows as opposed to the bulk of the SFD. We did this because we noticed a steep increase in slope at smaller diameters of ~50–90 m before the SFD again matched an isochron, which is similar to what we observed in the overall SFD for Arsia's caldera (Fig. 8). We attribute this enhancement to secondary craters, as discussed above.

3.3. Ascraeus Mons

Ascraeus Mons is the northernmost of the three Tharsis Montes, residing at 12°N 255°E. The volcano rises 15 km above the surrounding surface and 18 km above the martian datum surface. It has an average diameter of 350–400 km. The caldera complex of Ascraeus (Fig. 2c) is characterized by a large, central caldera with an average diameter of ~25 km (total area 508 km^2). It is surrounded by four additional calderas, one each to the northeast, northwest, southeast, and southwest. The southwest caldera (caldera 5 in our mapping) is surrounded by two terraces. Though each terrace was initially thought to be a collapse feature and so should have the same age as each other and the caldera, our crater ages show the upper to be approximately twice as old and statistically distinct from the main floor of caldera 5 for diameters $D < 110$ m; this was likely missed in previous studies because they were incomplete to the decameter scale. Because the lower terrace and the main caldera 5 had similar ages, we combined them in our final mapping and age determinations. It is still possible these represent collapses of one originally larger caldera, but such an interpretation would need to account for the significantly different ages.

Caldera 1 did not parallel the isochron slopes throughout most of its range, instead having a slope slightly greater than the isochrons (indicating possible contamination by secondary craters) (Fig. 5c). We were able to fit it between 80 and 160 m to the 250 Ma isochron. Caldera 2 was nearly an ideal case, closely matching the 320 Ma isochron throughout its entire extent, 55–225 m. Caldera 3 started on a ~570 Ma isochron at ~300 m diameter craters but it rose to lie on the 1.1 Ga isochron between 67 and 135 m. Caldera 4 was more ambiguous, starting at the large diameter (500 m) end around an age of 3.2 Ga, but quickly crossing several billion years of crater density to 730 Ma between 65 and 165 m. Combined, calderas 5 and 6 have a relatively small area and few craters, but they seem to parallel two distinct isochrons – 320 ± 100 Ma at the larger 120–170 m range and 230 ± 30 Ma at sizes of 75–90 m. Finally, the upper terrace, caldera 7, appears to have a younger age at larger crater sizes of 230 Ma, and then an older age of 570 Ma at sizes of 50–80 m. This older age at a larger size is one of three instances (Arsia Mons, this, and Olympus Mons) resulting from probable contamination from undistinguished secondaries. See discussion of Arsia Mons in Sections 3.2 and 8.1.

Our derived crater ages agree with Neukum et al. (2004) and Werner (2009) for caldera 4 (the southwestern caldera), for which we estimate the age as 730 ± 60 Ma, Neukum et al. (2004), 800 Ma, and Werner (2009), 785 Ma. Within a ±20% uncertainty for the for-

mer comparison, these ages are consistent. Otherwise, our ages are consistently older than determined in the other two papers. Caldera 1 is older by a factor of 2.5, caldera 2 a factor of 1.5, and caldera 5 is older by a factor of 2.4; the absolute age differences here are only 100–150 Myr, though. By far, the largest disagreement is caldera 3, the caldera to the northwest. We calculate an age of 1060 ± 50 Ma, while Neukum et al. (2004) and Werner (2009) derive an age of approximately 400 Ma. We discuss potential reasons for discrepancies in Section 10.

3.4. Biblis Tholus

Biblis Tholus is an asymmetric volcano located at 2.5°N 235.5°E. The volcano rises 4 km above the surrounding terrain though the caldera sinks down to a remarkable 5.5 km below the rim. Biblis is a highly asymmetric volcano even after the local topography and likely burying of its eastern flanks are taken into account. Its present-day major axis is 170 km and minor axis is 120 km, and the caldera is located in the eastern third with shallower flanks to the west.

The caldera of Biblis Tholus is somewhat complex, though at first glance it is a simple collapse structure, as shown in Fig. 2d. The northern walls show evidence of heavy alluvial–colluvial mass wasting, covering part of the caldera floor and thus confusing crater counts in this region. One of the main features of the caldera is a central collapse feature nearly 10 km across which likely represents the last central vent of primary volcanism for the volcano – a possibility also supported by our derived ages. Topographically, the northern half of the caldera is lower than the southern half, and it also shows textural and graben features not observed in the southern half.

In the SFDs for the calderas of Biblis Tholus, we found one of the most severe cases of resurfacing out of the 20 volcanoes we analyzed (Fig. 5d). Determining which diameter bins to use to fit isochrons was very difficult and highly subjective. Our method for the main central vent was to use the largest diameter bin that contained 3 or more craters. The resulting age was 480 ± 270 Ma, and we interpret this as a maximum surface age; by "surface age" we are not necessarily indicating formation age, but rather the most recent event to cover it, keeping in mind it sits in a steep topographic low. Calderas 2 and 3 were fit as per Section 2.3, which led to model ages $3.20^{+0.19}_{-0.67}$ Ga and 2.10 ± 0.44 Ga, respectively. Statistically, these are the same age, and if one were to choose a different range over which to fit the SFDs, the ages would be closer. Caldera 4 was fit to the two largest diameter size bins that had $\geqslant 3$ craters, which resulted in a model age of $3.35^{+0.19}_{-1.45}$Ga. This is also statistically identical to calderas 2 and 3.

If we combine all four calderas into a single surface, we calculate a model age $3.37^{+0.14}_{-0.67}$ Ga when fitting between diameters 500 and 870 m. The only comparable research on the caldera of Biblis Tholus that has been published is from Werner (2009), who calculated an age of 3.68 Ga for the entire caldera. This is older than our derived age, though Werner does not provide uncertainties in the published measurements. If we apply a conservative ±10% uncertainty to Werner (2009), then we agree statistically, though we note that Werner's age also includes the volcano's flanks.

3.5. Ceraunius Tholus

Ceraunius Tholus is a volcano at 24°N 262.5°E with flanks that are characterized by the presence of a dense network of fluvial channels arranged in a radial pattern with respect to the volcano's summit, similar to its northern neighbor Uranius Tholus. The structure rises 6.5 km above the surrounding surface and contains three distinct calderas – the upper two elevated about 800 m above the main central one. The tholus is elliptical, having a major axis ~140 km and minor ~100 km, although the caldera is centrally located unlike that of the similarly elliptical Biblis Tholus.

We mapped four separate calderas on Ceraunius' summit, as shown in Fig. 2e. The first is the main collapse caldera. It is uncertain whether the second represents a separate volcanic event based on the mapping, but it has a distinct topography rising above the primary caldera, and its surface roughness is very different. This raised block could be the relic of the volcanic cap broken by the events responsible for the formation of the main caldera. Calderas 3 and 4 are both hemispherical and are to the north of the primary caldera.

Ceraunius Tholus' calderas reveal an archetypal case in interpreting SFDs (Fig. 5e). Calderas 3 and 4 between diameters ~160–230 m show Hesperian ages of $3.59^{+0.05}_{-0.08}$ Ga for caldera 4 and $3.41^{+0.13}_{-0.62}$ Ga for caldera 3, likely representing distinct eruption events early in Mars' history. We do note that these are statistically distinct, despite the northern margins of calderas 3 and 4 residing along the same arc and having an alternative interpretation that caldera 3 collapsed to a lower elevation than caldera 4 after they formed together; we prefer not to make assumptions about this caldera since its statistical significance could be complicated by small-number statistics at the larger diameters we used. However, the interpretation that the two calderas are distinct is bolstered by the fact that caldera 4 lies along ~2–3% of the geometric saturation for diameters 150–300 m; if it is actually saturated, then our derived age is a minimum because further crater accumulation is not possible. At smaller diameters – until about $D < 70$ m – the SFDs are nearly flat, representing a resurfacing event. At smaller diameters, the SFDs again parallel an isochron at nearly identical ages of 590 ± 50 Ma and 510 ± 70 Ma for calderas 4 and 3, respectively.

While calderas 3 and 4 are old, calderas 1 and 2 are much younger. It is possible they have the same original age and caldera 2 is a deposit within caldera 1 that was placed very soon after activity ceased within caldera 1. We derive a split age of 630 ± 140 Ma for caldera 1 at large diameters 160–250 m and a statistically distinct 470 ± 40 Ma for 100–125 m. Caldera 2 has a model age of 400 ± 70 Ma for diameters 70–110 m. Within the counting statistics, these ages match the age at which calderas 3 and 4 began to re-accumulate craters.

The tholus has several features that suggest calderas 3 and 4 may have held paleolakes that drained into Rahe Crater to the immediate north (Fassett and Head, 2007). Evidence to suggest this includes fluvial drainage channels that emanate from caldera 3 primarily, run down the north face of the tholus after merging into a single channel, and then breach Rahe's wall and terminate in a topographically elevated region of deposits at the mouth of the channel that opens into Rahe crater (Fassett and Head, 2007). The deposits are positioned like a delta, but they are morphologically dissimilar to other identified deltas on the planet (Di Achille and Hynek, 2010). A different plausible interpretation is that they are simple lava deposits, though this would make the paleolake interpretation of Fassett and Head (2007) less likely. However, this would not change the chronology.

We have age-dated the relevant features in support of the chronology of events discussed above – whether the fluvial morphologies are volcanic or aqueous in nature does not change this. We have dated the flanks of Ceraunius by using $1.5 < D < 4$ km craters to $3.75^{+0.06}_{-0.09}$ Ga, though we note that the $0.6 < D < 1$ km range has a well-defined and distinct isochron age of $3.58^{+0.03}_{-0.04}$ Ga (Werner (2009) determined a crater retention age of 3.74 Ga). Both of these are fully consistent with the ages we derived for calderas 3 and 4. We date Rahe Crater to $3.68^{+0.05}_{-0.07}$ Ga, placing it roughly 100–200 Myr older than the surface of calderas 3 and 4, though this is still consistent with our interpretation that we are dating the last

volcanic activity from each caldera, and it is also consistent with the older age at larger diameters for the volcano's flanks. The deposits at the base of the channel within Rahe have a model age $3.42^{+0.10}_{-0.32}$ Ga, placing it at statistically the same age as caldera 3 and statistically younger than the crater floor – a good find that helps validate our methods of age dating using small craters over small areas. The narrow channel floor itself was more difficult to date and has a model age of 210 ± 100 Ma. While this is significantly younger, it can be explained by mass wasting within the originally steep channel walls over time even though we only used the floor for crater counts. The floor of Rahe shows the same evidence of erosion as calderas 3 and 4, with its younger age roughly fitting a 260 ± 10 Ma isochron.

In sum, and as illustrated in Fig. 9, our derived chronology for the Ceraunius Tholus region has most of the volcano built by ~3.75 Ga with Rahe Crater emplaced ~70 Ma later. Caldera 4 was last resurfaced ~3.59 Ga with caldera 3 resurfaced ~180 Ma later. The deposits on the floor of Rahe have an age matching caldera 3's age. The volcano was relatively quiet for the next 3 Gyr or it had ongoing but subsequently erased activity, with calderas 1 and 2 showing ages ~400–500 Ma and small-crater resurfacing ages in calderas 3 and 4 just slightly older, ~500–600 Ma.

3.6. Jovis Tholus

Jovis Tholus is a volcano centered at 18.5°N 242.5°E. The structure is probably the smallest volcanic tholus on Mars, rising only 2 km above the surrounding surface. It shows a complex collapse structure with the deepest caldera dropping the full 2 km below the highest point. The tholus averages 50 km across. The caldera structure of Jovis is open to interpretation: We mapped out seven distinct calderas (Fig. 2f), we later combined calderas 3 and 4. The main caldera 1 empties into the surrounding terrain on its west edge, while 2–4 appear to be terraces above it. Calderas 5–7 are somewhat distinct, appearing to represent successive stages of volcanism relative to each other, but before the main caldera.

Age dating the different calderas of Jovis was complicated by the small-diameter fall-off seen in the SFDs, often after only the first few larger-diameter bins (Fig. 5f). The main caldera 1 has the age 2.13 ± 0.38 Ga by fitting diameters 210–370 m. Calderas 2–6 were less clear, and our estimates range from 400 Ma to 2.78 Ga (see Table 2). Caldera 7 had a derived crater age of 1.76 ± 0.44 Ga over the 220–320 m diameter range. With the large uncertainties and ill-behaved SFDs, we are hesitant to state these ages with any certainty other than calderas 1, 2, and 7. Overall, caldera 5 does appear to be the youngest based upon the overall cumulative crater density, with the joint 3/4 the second youngest, while caldera 6 is the oldest. Much of the uncertainty is due to the small numbers of craters (as few as 13) found in some of the calderas (see Table 1).

3.7. Olympus Mons

Olympus Mons is aptly named because it is the tallest volcano in the Solar System, rising 21 km above Mars' datum and up to 24 km above the surrounding plains. It is the westernmost of the Tharsis volcanoes with its center at 18.5°N, 226°E. The main volcano averages 550 km across, though beyond the high scarps at its present-day margin, material from it extends over 1000 km from the summit. Typically, Olympus Mons has been mapped with five calderas at its summit (*e.g.*, Neukum et al., 2004). Following our liberal mapping, we identified six calderas, splitting one of the middle calderas by following an arcuate ridge, shown in Fig. 2g.

Nearly all of the SFDs of the calderas on the summit of Olympus Mons represent an interesting case of split ages where the younger age is at larger diameters and the older age is at smaller diameters (Fig. 5g) (this is one of three cases where we observe this, the other two being Arsia Mons and caldera 7 of Ascraeus Mons). This is likely a feature of secondary cratering combined with erosion and/or incomplete crater identification at small diameters. There is possible evidence for secondary craters in the distribution of craters on the ground, but it is not nearly as conclusive as Arsia Mons' caldera (Fig. 7).

In general, the ages were fit over diameters ~140–300 m, while the "older ages" (laying on an older isochron) are over ~70–130 m. Because these likely do not represent an actual older age and are the results of secondary crater contamination, we will only quote here the "younger" ages. The figure legend (Figs. 2g and 5g) contains both. Caldera 1 dates to 240 ± 70 Ma; caldera 2 140 ± 50 Ma; caldera 3 to 240 ± 40 Ma; caldera 4 to 260 ± 70 Ma;

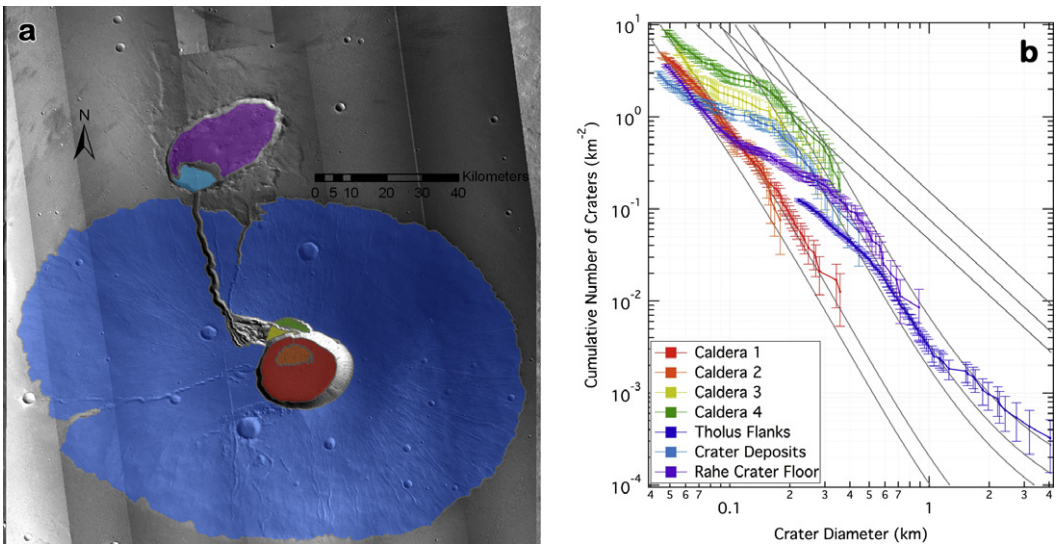

Fig. 9. Part (a) shows the geologic mapping and larger context of Ceraunius Tholus, including all mapped regions. Part (b) contains the SFDs of the four calderas, Rahe Crater, the deposits within the Rahe Crater, and the tholus itself. The channel discussed in the text is not shown in the SFD due to its likely anomalous results that we attribute to billions of years of infilling. Isochrons shown are 0.25, 0.50, 3.4, 3.6, and 3.75 Ga. Due to space considerations, the legend does not contain fitted ages but they are included in the text. Shallower grey lines are 3%, 5%, and 10% geometric saturation.

caldera 5 to 250 ± 40 Ma. Although workers typically combine calderas 3 and 4 into a single unit, our crater counting statistics point to different ages for each. Finally, caldera 6 has a single age of 140 ± 20 Ma, making it the youngest on Olympus Mons, and it is also the third youngest age that we found (older than Pavonis and Arsia, though all are statistically within each other's uncertainties). We note that over the diameters fit – which was nearly the entire available range – the SFDs were extraordinarily good fits to the isochrons, paralleling them almost exactly with minimal scatter.

Comparable, statistically-identical ages were found by Neukum et al. (2004), who found ages that agree with all of our younger ages for every caldera except for caldera 5. For caldera 5, they derived an age of 140 Ma, approximately 60% as old as our younger age for that caldera. Overall, Werner (2009) dated the entire summit caldera complex to 101–215 Ma, which is a reasonable match to Neukum et al.'s (2004) average. If we combine all craters from the summit and age-date that, we arrive at an age of 230 ± 30 Ma which is in statistical agreement.

3.8. Pavonis Mons

Pavonis Mons is the central of the three Tharsis Montes, situated at 1°N 246.5°E. It rises 9.5 km above the surrounding surface and 14 km above the martian datum. The volcano averages 300–350 km across. Geomorphologic mapping of Pavonis' summit calderas is uncomplicated. There is one large caldera approximately 80–85 km in diameter and another, smaller caldera 30 km across superimposed on its southwest margin (Fig. 2h). We did not date the two much smaller calderas with a total area 10.9 km^2 located at the northern edge of the main one. One interesting feature of the main caldera is that on its western side it is bounded by a scarp and falls below the surrounding surface, having an obvious rim. On the eastern side, the margin of the caldera is marked by a semicircular convex ridge, rising above the surrounding surface. This is interpreted to be the result of the most recent lava flows overtopping the rim but being viscous enough to maintain a competent flow.

Determining a model age for Pavonis' caldera 1 was straightforward, and we used diameters in the range of 93–200 m to derive an age of 130 ± 20 Ma – tying Arsia as the youngest age of a caldera that we found (Fig. 5h). Caldera 4 showed more evidence of resurfacing in the down-turn in the SFD for $D < 300$ m. We fit from 300 m to 600 m and derived a model age of 860 ± 170 Ma. The relatively large uncertainty is due to scatter around the isochron at those diameters. Our age for caldera 1 compares reasonably well with Werner (2009), who derived an age of 82 Ma. If we attach a ±20% uncertainty to the quoted age, we nearly agree. Comparison with the older caldera does not agree, where Werner derived an age dating to 367 Ma – less than half our age. In comparing published SFD data and examining crater morphologies, we believe this is due to Werner under-counting the craters in the caldera. This caldera age is one of the largest discrepancies between our work and hers.

3.9. Tharsis Tholus

Tharsis Tholus is a small volcano that is the easternmost of the Tharsis edifices, its center located at 13.5°N 269°E. It is relatively small, rising a maximum of 7.5 km above the surrounding surface, with its base averaging approximately 140 km across, though the shape is irregular and does not have a simple footprint. Like Jovis Tholus, the volcano shows significant signs of collapse with its east-northeastern quarter slumped by over ~3 km, its western fifth similarly collapsed by ~1.5 km, and the deepest caldera dropping approximately 6.5 km below the highest point. Mapping Tharsis Tholus' complex again illustrates our liberal approach, leading to the identification of seven calderas within the summit (Fig. 2i). Caldera 2 is separated from the first due to the fact it appears to be a newer surface likely as a result of the mass wasting deposits from the western wall. Calderas 3–7 are topographically or geographically separated terraces that we cannot obviously link together. However, we did combine calderas 3 and 4 in our final analysis due to their rather small sizes and possible genetic link.

Fitting isochrons to the SFDs for the various calderas was rather difficult as they are nearly flat instead of following the isochron slopes (Fig. 5i). We attribute the deficit to resurfacing events. We report a few examples and direct the reader to Table 2 for a complete listing: In dating the calderas, we attempted to use the largest few diameter bins for each caldera that approximately paralleled an isochron. Although we provide formal uncertainties per Section 2.4, we believe that this is another case where the actual uncertainties are likely larger due to the marked resurfacing evidenced by the SFDs. With those caveats, we fit an age of $2.46^{+0.63}_{-0.75}$ Ga to caldera 1, and $3.24^{+0.17}_{-0.62}$ Ga to caldera 2. Already, geologically we see problems in our age fits because cross-cutting relations indicate caldera 2 overlies 1 as a result of collapse and not volcanism, indicating it should be younger. A possible explanation – besides the uncertainties in the ages actually overlapping – is that caldera 1 collapsed further after 2 formed, erasing many of the craters emplaced on it, and then it began to re-accumulate them. This is somewhat supported in that the largest two bins – craters $D > 600$ m – for caldera 1 indicate an older age than caldera 2. Previous published work for just dating Jovis' calderas does not exist, so we cannot turn to those for possible reconciliation.

3.10. Ulysses Patera

Ulysses Patera is next to Biblis Tholus, centered at 3°N 238.5°E, and it rises only 1.5 km above the surrounding surface. The edifice is 95 km across on average. A rather unique feature of this volcano is that the floor drops an impressive 2.5 km below the summit and averages about 1 km below the surrounding surface. The caldera is also one of the largest in diameter relative to the volcano's extent, slightly more than 50% its width.

Mapping the caldera of Ulysses was complicated only by the two relatively large craters superimposed on it with their layered ejecta blankets (Fig. 2j). The latter were not included in the final mapping and therefore we only considered the region of the caldera not covered by the ejecta. Our analysis (Fig. 5j) shows some resurfacing at diameters smaller than ~250 m, but the SFD shows no evidence of any contamination by secondaries from the two large craters; this is somewhat expected because we do not anticipate seeing significant secondaries until at least one crater diameter from the rim. We fit an isochron to the caldera that dates it to 1.42 ± 0.30 Ga.

3.11. Uranius Mons

Uranius Mons contains the third largest caldera complex on the planet – behind Alba Mons and Arsia Mons – with a caldera complex area of ~6260 km^2. Uranius Mons is located at 26°N 267°E, just east of Uranius Tholus and Ceraunius Tholus. It rises a maximum of 4 km above the surrounding surface, and it averages ~250 km across. The floor drops to only ~200 m above the surrounding surface (~3.8 km below the rim).

Geomorphologic mapping of Uranius Mons was made difficult by the poor data quality of the available CTX imagery (Fig. 2k). While there is complete CTX coverage of the volcano, just over 50% of the caldera is only covered by very grainy images that have not been re-imaged at the time of this writing (May 2010). This reduced the usable area of Uranius Mons' caldera complex to

3183 km^2, as reflected in Table 1. We mapped the region with seven different calderas, the first two segregated by a topographic ridge, and the third and fourth based on textural characteristics. Calderas 5 and 6 are tilted regions raised above the main summit and trending towards the central region of the volcano. The layered ejecta blanket of the large crater embedded in the eastern half was excluded from the final units. Caldera 7 is a terrace above caldera 5 but below the surrounding rim. We note that, while liberal, this was also a pragmatic approach to mapping similar to Alba Mons, where we did not attempt to trace original caldera margins but instead concentrated on attempting to delineate eruptive events.

Dating Uranius Mons was clear for some calderas and not for others (Fig. 5k). Of primary interest, calderas 1 and 2, with well constrained model ages of $3.19^{+0.10}_{-0.19}$ Ga and $3.43^{+0.07}_{-0.05}$ Ga, respectively, lie on their respective isochrons with minimal deviation. Caldera 1 shows signs of resurfacing at $D < 150$ m. Caldera 2 shows a possible increase due to secondaries between 250 and 300 m, but below that has significant signs of resurfacing. However, for $D < 60$ m, the SFD changes slope again and appears to nearly parallel a production function. Empirical saturation provides an alternative explanation to resurfacing since the crater population SFD matches 1.4–1.5% of geometric saturation. Using this as an explanation is complicated by the SFD for caldera 6 easily breaching that empirical saturation line. The remaining calderas are more ambiguous, and we list the results in Table 2.

Werner (2009) also attempted to date the summit caldera complex of Uranius Mons, though Werner dated the entire region as one caldera. The paper's age of 3.7 Ga is older than any of our derived ages, though if we attach a ±15% uncertainty to the estimate we would be in statistical agreement over much of it.

3.12. Uranius Tholus

Uranius Tholus is just north of Ceraunius Tholus and west of Uranius Mons; its center is at approximately 26.5°N 262.5°E. It rises 2.5 km above the surrounding plains with an approximate diameter of ~60 km. Its flanks are characterized by several channels radiating from its summit, similar to its southern neighbor, Ceraunius Tholus.

The summit of Uranius Tholus contains two clear nested calderas shown in Fig. 2l. Their SFDs (Fig. 5l) show significant evidence of resurfacing at diameters smaller than ~300 m. We date them to statistically-identical ages – $3.57^{+0.06}_{-0.09}$ Ga and $3.56^{+0.06}_{-0.10}$ Ga. Due to the closeness in ages, it is likely that the two calderas formed originally from the same eruptive event, and caldera 1 is a subsequent collapse from the original elevation of caldera 2. The SFD of caldera 1 shows a decrease in slope at diameters smaller than ~300 m, where it is statistically older than caldera 2. This could be due to erosion, but the crater population lies near the 1.4% geometric saturation line so saturation may also play a role. Similarly, caldera 2 shows a decrease in slope that closely matches an empirical saturation of ~1% geometric, and this match is over the 100–300 m diameter range. Attributing the overturn to empirical saturation or to a process that is not volcanic- nor crater-related is not a distinction we can make with this work. Werner (2009) dates both calderas together to be 3.9 Ga, significantly older than this analysis. However, if we attach a conservative 10% uncertainty to the age estimate, than we do statistically agree.

4. Syrtis Major

Between Arabia Terra on its west and Isidis Basin on its east, Syrtis Major is a large volcano composed of two main caldera complexes – Meroe Patera to the south and Nili Patera to the north (Fig. 3a and b). The flows of Syrtis Major roughly date to the Hesperian epoch of Mars, around 3.5 Ga (Tanaka et al., 1988). They overlie Nili Fossae and breach the western rim of Isidis. Syrtis Major has an approximate diameter of 1200 km (~1/3 Tharsis' extent).

The volcanism of Syrtis Major was probably partly explosive, typically characterized by far-reaching flows from the caldera and little topographic difference between caldera floors and their rims. However, the low slopes and long still-visible lava flows emanating from the calderas today indicate that a significant part of it was built effusively. The edifice reaches a maximum elevation of 2 km above Mars' datum. The caldera complex drops to ~500 m above that surface, while the calderas themselves drop an additional 300 m to reside ~200 m above the MOLA datum. This is likely due to a broad collapse into a vast, evacuated magma chamber.

In the next two sub-sections, we derive the ages for Meroe and Nili Paterae (Fig. 6a and b), and we determine that the surface of Nili Patera post-dates Meroe by up to 1.5 Gyr. We speculate on three possible reasons for this observation. The first is that Nili and Meroe were fed by a single plume that migrated over time towards the north, shutting off volcanism in Meroe and starting it in Nili. A second possibility is a branching vent fed both Meroe and Nili, and the one under Meroe died out first. A third possible explanation is that there were simply two original vents, the southern one exhausting its magma supply before the northern. It is also possible, although unlikely, that weathering patterns are different over the ~3° distance that separates the two and Nili endured more recent resurfacing than did Meroe.

4.1. Meroe Patera

The vent towards the south, Meroe Patera, is centered on 7°N 68.5°E and is more circular than its counterpart to the north. We were very liberal in mapping the caldera, identifying eight separate events and regions based upon topography and texture. However, after a second look at the mapping and the indications from later-determined ages, we combined both calderas 2/4 and calderas 6/7 into single events for SFD and age-determination purposes.

Even with these combinations, age-dating Meroe's calderas was complicated by the resurfacing and erasure of its smaller craters. Calderas 1–4 were relatively easy to date: 1 dates to $2.9^{+0.4}_{-0.8}$ Ga, caldera 2/4 to 2.9 ± 0.5 Ga, and caldera 3 to $3.0^{+0.3}_{-0.7}$ Ga. We note that all of these are statistically identical. Caldera 5 may be as old as 1.4 Gyr based on the largest two diameter bins, but the 230 ± 90 Ma isochron provides the best fit. Calderas 6/7 have a split age, the diameters 500–800 m yielding a 3.8 ± 1 Ga age while diameters 300–400 m show a 3.6 ± 0.1 Ga model age. Caldera 7 spans over 3 Gyr of isochrons, but about half of the bins lie on the 2.0 ± 0.7 Ga isochron with little scatter.

The only comparable work on Meroe's caldera was done by Werner (2009), who found an overall age of 3.73 Ga for the entire caldera complex. Within any reasonable uncertainty on this number (*i.e.*, 5%), we are in statistical agreement.

4.2. Nili Patera

Nili Patera, north of Meroe, is a heavily modified caldera that is centered at 9°N 67°E. A significant portion of its southwestern surface is covered by vast, dark dune and ripple fields – the only such instance in all of the calderas we examined – making mapping somewhat difficult. These aeolian deposits are relatively young and obscure the underlying features, making the determination of their crater ages difficult. We speculate they may be due to weather patterns from the adjacent Isidis Basin (Rafkin and Michaels, 2003).

We initially identified five separate calderas, but we merged calderas 3–5 into a single event for purposes of age dating based

both upon a re-examination of the contacts and on their individual ages. Following the same techniques as with the other volcanoes, we determined a split model crater age of $3.0^{+0.2}_{-0.5}$ Ga and $3.6^{+0.1}_{-0.2}$ Ga for caldera 1, based on craters ~170–300 m and 350–500 m, respectively. Caldera 2 has an age of 1.6 ± 0.5 Ga, while the combined calderas 3–5 have a model age dating to 2.0 ± 0.3 Ga.

5. Elysium complex

The Elysium region is located near the eastern rim of the giant Utopia Basin and consists of three relatively clustered volcanoes amidst fairly young terrain. The complex's largest, westernmost volcano is eponymously named, while to its northeast lies Hecates Tholus, and to the southeast is Albor Tholus. Farther south lies Apollinaris Mons, though we address that separately in Section 6 for reasons made clearer in Section 9.

5.1. Albor Tholus

Albor Tholus, the southernmost of the three Elysium volcanoes, is centered around 19°N 150.4°E. It rises ~3.8 km above both the surrounding plains and the martian datum. It has a diameter of approximately 165 km. Mapping the summit calderas of Albor seems, at first glance, relatively clear with a smaller, lower elevation caldera to the north, emplaced within a larger caldera (Fig. 3c). However, to be consistent with the mapping of Neukum et al. (2004) and based upon the presence of ridges and surface textures, we segregated the larger caldera into three separate ones.

Resurfacing plagued our age determinations for Albor (Fig. 6c). We estimate the age of caldera 1 to be 1.50 ± 0.36 Ga based upon the 110–280 m range; at smaller diameters the slope is shallower, matching ~1% geometric saturation. Caldera 2 has a model age of 940 ± 270 Ma for diameters 175–250 m. Caldera 3 has an age relatively close to the other two, 1.01 ± 0.31 Ga over 125–220 m. Finally, we derive an ancient age for caldera 4 of $3.54^{+0.07}_{-0.13}$ Ga over the diameter range 380–475 m.

Compared with the work of Neukum et al. (2004), our model crater ages are fairly different. For caldera 1, their age is 500 Ma, 1/3 ours. We barely statistically agree to within their standard 20% uncertainty with caldera 2, where they derive an age of 600 Ma. Caldera 3 is the same case, though their age is older at 1.6 Ga, barely within the joint uncertainties. Finally, caldera 4 is completely different, where they derive an age of 2.2 Ga, placing it in the Amazonian while our age of $3.54^{+0.07}_{-0.13}$ Ga places the caldera in the Hesperian epoch. This caldera complex represents our largest discrepancy with the work of Neukum et al. (2004). In reconciling these, Werner (2009) is not helpful as the entire caldera complex was dated as one, assigning it an age of 1.6 Ga.

5.2. Elysium Mons

Elysium Mons is the tallest of the three in this region, and it is the farthest west at 25°N 147°E. The volcano rises to a maximum of 14 km above the martian datum, though it is difficult to estimate where precisely the volcano's base lies due to the very steep ~8.3° slope for ~50 km from the summit that breaks to a shallower ~5.3° for ~100 km from the summit, and then a much shallower, ~0.6° slope that continues for an additional 350–600 km. If we take the maximum extent, then the volcano rises 18 km above the surrounding surface.

The summit of Elysium Mons is capped by a single main caldera (caldera 2) and two ancillary ones (Fig. 3d). Caldera 1 is fully embedded within caldera 2, and we chose to separate it due to its topographic distinction since it lies below the surrounding surface of caldera 2. This is in marked contrast with our mapping of Alba Mons and Uranius Mons, where we only identified the last eruption episodes due to an inability to distinguish individual historic eruption regions. Caldera 3 for Elysium is a thin crescent-shaped terrace above caldera 2, following it about 60% around.

When dating the three calderas, we used crater diameters approximately in the range 100–250 m for all three (Fig. 6d). Caldera 1 had a model crater age of $3.1^{+0.2}_{-0.6}$ Ga, caldera 2 $2.8^{+0.2}_{-0.2}$ Ga, and caldera 3 was $3.2^{+0.2}_{-0.6}$; Ga. We note that these are statistically identical and interpret them as likely being from the same eruptive episode. A possible history for the three is the last eruptive event created a caldera that extended through calderas 2 and 3, and it was at the elevation of caldera 3. Subsequent collapse brought calderas 1 and 2 to the present day elevation of caldera 2, and collapse from possible evacuation of a magma chamber drained support from caldera 1, causing slight subsidence.

Elysium represents an interesting case of empirical saturation of craters. Caldera 1's slope matches an empirical saturation level of 3.5% geometric, while caldera 2's is fully 4.2% geometric saturation at smaller diameters. This represents the highest level we observed of any region we studied in this work. Caldera 3 is roughly 3% of geometric saturation at larger diameters (as large as ~125 m) though it falls below this at $D < 100$ m, likely due to resurfacing and mass wasting since it is a narrow strip no wider than 500 m.

Werner (2009) also age-dated Elysium Mons, though the entire summit was dated as a single caldera. The derived age of 3.49 Ga statistically agrees with our ages if we apply a conservative ±10% uncertainty. In contrast, Pasckert et al. (2010) arrived at a much younger 1.48 ± 0.20 Ga for the combined calderas 1 and 2. However, they did not include approximately half of the craters in their analysis. Their argument is that they are likely to be secondary craters (personal communication), though upon morphologic examination we do not see such evidence. One could make a statistical argument to exclude a certain fraction of the total craters counted due to them being probable secondaries, but we do not think one can dismiss regions of the surface from the initial mapping as well as omit craters that are fully within the designated mapping region when they do not display any standard morphologic secondary crater characteristics (Shoemaker, 1962; Oberbeck and Morrison, 1974), such as entrainment in ejecta or clusters. Subtraction of presumed secondaries from a model crater population could be a reasonable approach, but that was not done in this case.

5.3. Hecates Tholus

Hecates Tholus is the northern volcano of the trio that comprise the Elysium complex; it is centered at 32.5°N 150°E. It has a summit that lies ~7 km above the surrounding terrain and an average diameter of ~190 km. Mapping the summit calderas of Hecates was relatively easy (Fig. 3e). There are four obvious concentric levels of calderas at the summit, though we followed Neukum et al. (2004) and subdivided the second-highest into two distinct calderas due to a ridge that lies between them. The total area of the summit calderas is only 66.4 km^2, and we were only able to identify 145 craters over all five calderas from CTX imagery.

This number is woefully inadequate to obtain statistically significant ages (Fig. 6e), though we performed the exercise for completeness as well as a resolution verification case study. We also compare our ages with Neukum et al. (2004) and Werner (2009), though the ages reported are identical so we will only list the comparison once. Caldera 1 was dated based on the two largest bins, ~100 m in diameter, and fits to 200 ± 110 Ma. Compared with an age of 322 Ma, this is a reasonable match. Caldera 2 was fit between 70 and 105 m and we fit an age of 220 ± 80 Ma. This is also in reasonable agreement with Neukum et al. and Werner's age of 90 Ma. Using all three diameter bins of caldera 3, we date it to 1.01 ± 0.46 Ga, though this is approximately 3–4 times as old as

the 250–300 Ma comparison age. Caldera 4 was the most significant difference. We used our three largest diameter bins, 220–270 m, and derived an age of $3.53^{+0.11}_{-0.57}$ Ga. In contrast, they derived an age of 110 Ma by dating external lava flows in addition to the calderas to derive what they considered statistically more meaningful results. We consider our method of dating only the calderas to be more reliable in this case. Additionally, our SFD for caldera 4 is among the best defined for this region, for it shows a good fit to the 3.53 Ga isochron. Finally, caldera 5 is also not in statistical agreement. We used a range of 185–210 m to fit a model crater age of $2.67^{+0.59}_{-1.00}$ Ga, while they calculate an age of 1.01 Ga. Interestingly, from approximately 90 m to 200 m, the crater frequencies for calderas 4 and 5 lie on the 1% geometric saturation line, though we are not convinced that this is the reason for the shallower slopes here.

While Hecates Tholus fails as an overall useful location for our technique of crater-age dating volcanic calderas, it is small enough to serve as a case study for our statistical completeness of craters. We obtained the HiRISE image PSP_005259_2120_RED, which covers ~76% of the summit's calderas. At a resolution of ~25 cm/pix (compared with 10 m/pix for our CTX mosaics) and outlining crater rims at a resolution of 1 vertex every 5 m (compared with 25 m for CTX), we performed crater counts independent of the counts we did using CTX images. The results (calderas 3 and 5 shown in Fig. 10) show that we were statistically complete for craters to diameters ~60–70 m in the CTX data, helping to validate our claim of completeness to those diameters.

6. Apollinaris Mons

This volcano, centered at −8.5°N 174.5°E, is the only large, prominent, and isolated volcano on the planet that is visible today. It is southeast of the Elysium complex, and it resides near the crustal dichotomy boundary. Understanding it, the history of the region, and its eruptive past are important not only to the broader picture of Mars, but also to the interpretation of Mars Exploration Rover (MER) Spirit data since the Gusev Crater in which MER Spirit landed is covered by volcanic material likely from the nearby Apollinaris volcano (*e.g.*, Grant et al., 2004; Morris et al., 2008), though this has been debated (*e.g.*, Lang et al., 2010).

Apollinaris is characterized by a summit that lies ~4.5 km above the surrounding terrain though the main two calderas drop ~1.5 km below this. The volcano has an average diameter of 180 km. Geomorphologic mapping of Apollinaris' summit calderas was a complex undertaking, and it represents perhaps the one instance where we were fairly conservative (Fig. 3f). A sizeable region of this complex was excluded from the mapping due to its appearance of subsequent non-volcanic modification processes. We still identified six separate calderas, though due to their identical SFDs we later combined calderas 4 and 5 into a single unit.

The SFDs of Apollinaris Mons are a classic case, much like those of Ceraunius Tholus' calderas, of a resurfacing event. We observe an expected production function at larger diameters that match a relatively old isochron that likely represents the original crater population post-formation. We then observe a less steep slope in the SFD at intermediate diameters, representing a burial or erasure event that affected craters smaller than a certain size. After that event occurred, crater retention would resume, and we again observe a relatively steep production function slope that matches a younger isochron (Fig. 6f). For caldera 1, we calculate a model age of $3.57^{+0.03}_{-0.04}$ Ga. We note that the isochron is very clearly matched by the SFD over the range of ~500–800 m, below-which it matches the 1.1% geometric saturation line. Similarly, caldera 2 matches its isochron age of $3.52^{+0.05}_{-0.07}$ Ga over 400–700 m. Caldera 3 is more difficult to interpret. Between 1.08 and 1.53 km, the model crater age is the oldest we found – Noachian, at $3.93^{+0.06}_{-0.10}$. The SFD then goes nearly flat, increasing slowly, until $D < 100$ m, at which point it increases again to a model age that matches the increase in calderas 2, 4/5, and 6, of ~220 ± 20 Ma. The age of the combined calderas 4/5 fits the $3.77^{+0.04}_{-0.06}$ Ga isochron, while finally caldera 6 at larger diameters matches to $3.54^{+0.11}_{-0.52}$ Ga and 220 ± 30 Ma at smaller sizes. Over the brief range of 400–500 m, caldera 4/5 match 1.4% geometric saturation.

The comparable work done on Apollinaris was by Werner (2009), who lumped our calderas 1 and 2 into a single caldera, and then the rest into another. Werner's age for calderas 1/2 is 3.61 Ga, and the age for the rest is 3.72 Ga. With even the most conservative uncertainty estimate of ±3%, our ages statistically match.

As with a few of the other volcanoes studied herein, Apollinaris Mons is a good case study for exploring the role of secondary craters – both where they are produced and how they affect or do not affect crater size–frequency distributions. Apollinaris Mons contains three relatively large fresh impact craters on its summit – two are in caldera 1 and one is in caldera 2. They are 5.00, 6.14,

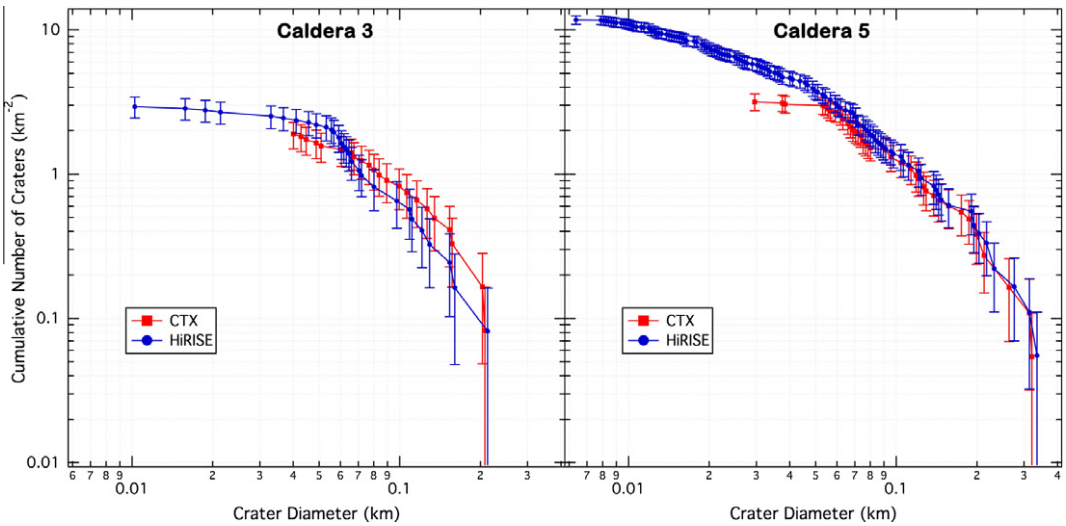

Fig. 10. SFD of Hecates Tholus' caldera 3 (a) and 5 (b), showing the comparison for HiRISE-based counts with CTX-based counts. We show these two calderas because they contain the most craters and they had the most complete HiRISE coverage (caldera 3 is 100% and caldera 5 is 98.6% covered). The results show that with independent resolution verification, we are statistically complete to the small diameters that we claim, roughly 50–75 m.

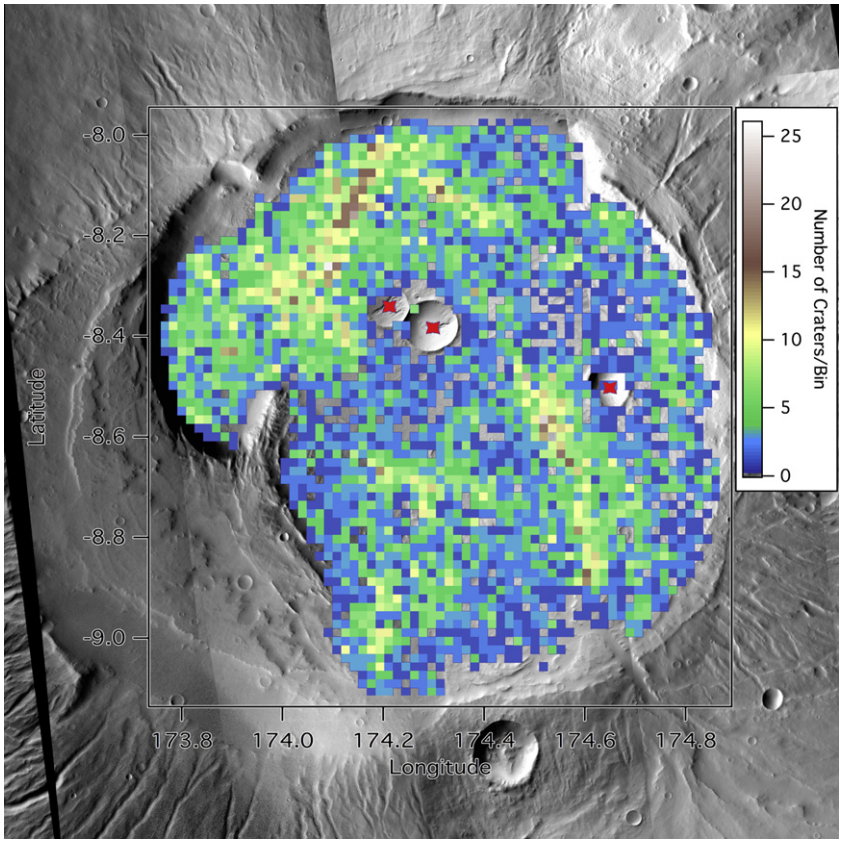

Fig. 11. A crater density plot of Apollinaris Mons' two main calderas. The three stars indicate the three largest >1 km superposed craters. Binning is 1 × 1 km. There are large, statistically significant enhancements of craters surrounding each of these large craters, indicating probable secondary fields. With standard $\sqrt{N}$ Poisson statistics, the general "background" levels of craters in these calderas averages 2–3 ± 1–1.5 craters per km^2. Within 2–3 crater diameters of the three large craters, the number of craters increases to 10–27 ± 3–5 craters per km^2, a statistically significant enhancement. Bins with 0 craters in it have been made transparent so the underlying base CTX map shows through.

and 5.23 km in diameter. A relatively close field of secondary craters surrounds all three. The only problem is that they are not morphologically obvious secondaries, unlike on the summit of Arsia Mons. In fact, the only way to tell that there are secondaries present is through a crater latitude/longitude density analysis (Fig. 11). This figure shows an increase of craters in an arc surrounding about 60% of the pair in caldera 1 and about 40% surrounding the one in caldera 2. These density increases are statistically significant, increasing from a background 0–5 (±0–2) craters per 1 × 1 km latitude–longitude bin to 15–25 (±4–5) craters per bin. In addition to secondaries being present in large numbers approximately 2–3 crater diameters away from each large primary (unlike the case of no obvious primary for Arsia Mons), we do not observe a statistical increase in the SFD for either caldera (also in contrast with Arsia). We explore the implications of these further in Section 8.

7. Northeastern Hellas Basin

Hellas Basin is the third- or fourth-largest impact feature recognized today on Mars (behind Chryse, Utopia Basin, and possibly the basin that formed the entire northern lowlands if it is of impact origin (Andrews-Hanna et al., 2008)). Hellas Basin dates roughly to 4.08 Ga, but it is still younger than all other large basins, save Argyre and Isidis (*e.g.*, Barlow, 1988; Nimmo and Tanaka, 2005). The impact event that formed Hellas must have induced massive melting that could have affected magma pockets around it and severely fractured the crust, acting as a catalyst for a large amount of local volcanism with crustal fractures acting as conduits. We support this scenario (proposed by *e.g.*, Peterson, 1978; and linked as the "Circum-Hellas Volcanic Province" by Williams et al. (2009)) because the only major volcanoes in the southern highlands of the planet surround Hellas: Two to the northeast – Tyrrhena Patera and Hadriaca Patera – and four to the south–southwest – Amphitrites Patera, Malea Patera, Peneus Patera, and Pityusa Patera. Unfortunately, due to a lack of CTX coverage we were only able to analyze Tyrrhena and Hadriaca. As we show below, the oldest model crater ages we found for the calderas is approximately 3.2–3.7 Ga, at least 400 myr younger than Hellas itself.

7.1. Hadriaca Patera

Hadriaca Patera is located within the rim of Hellas, centered around −30°N 93°E. It is characterized by a summit rim height that lies roughly 700 m below the Mars datum and a caldera floor that drops another 400–600 m. It is difficult to estimate the elevation above the surrounding surface because it resides upon the sloping walls of Hellas Basin, but we very roughly estimate that it rises ~1 km above the surrounding surface. The diameter of the patera averages ~270 km.

Geomorphologic mapping of Hadriaca Patera (Fig. 3g) was the most difficult and interpretative of the 20 we performed for this study although Apollinaris Mons' mapping was also one of the most difficult and subjective. We identified nine separate regions within the summit of Hadriaca by using a liberal mapping approach mostly based upon topographic relations and bounding ridges throughout. Upon re-examination after crater identification

had been completed, we combined calderas 3 and 4, and calderas 6 and 7, for a total of seven regions.

Overall, Hadriaca Patera's SFDs (Fig. 6g) show evidence of resurfacing, as with most we studied, though it was overall less severe than the worst cases (*e.g.*, Biblis, Jovis, and Tharsis Tholi). Caldera 1 was dated to 3.6 ± 0.1 Ga. Caldera 2 has a model crater age $3.3^{+0.2}_{-1.0}$ Ga. Calderas 3/4 combined have a joint age of 1.8 ± 0.5 Ga, and along with caldera 5 dated to 1.6 ± 0.5 Ga are the youngest. Calderas 6/7 date to $3.6^{+0.1}_{-0.4}$ Ga. Caldera 8 has a split age, where craters ~400–600 m in diameter indicate a model age of $3.6^{+0.1}_{-0.4}$ Ga, while ~200–300 m craters fit an age of 2.1 ± 0.7 Ga – statistically separate events, and possibly matching the event that formed calderas 3–5. A possible interpretation is that if those caldera regions formed in a single, separate volcanic event, lava ~20–30 m thick covered caldera 8, burying craters D < 200–300 m, after which it resumed crater accumulation. Finally, caldera 9 dates to $3.3^{+0.2}_{-0.6}$ Ga.

Comparing our results with others is somewhat subjective due to different mapping styles. Werner (2009) dated the entire caldera to 1.08–3.54 Ga. This easily fits within all of our caldera ages. Williams et al. (2007) also age-dated the caldera of Hadriaca. They divided it into two regions, their first caldera corresponding to our caldera 1, and their second roughly corresponding to our calderas 5–8. Our results agree well, where for the first and second they calculated an age of $3.5^{+0.1}_{-0.3}$. Their resurfacing ages are $2.6^{+0.3}_{-0.4}$ Ga and 1.5 ± 0.2 Ga, respectively, which roughly correspond with the ages of our calderas 3–5 and the resurfacing age of caldera 8.

7.2. Tyrrhena Patera

Tyrrhena Patera is located farther away from Hellas than Hadriaca, its center at −21.5°N 106.5°E. It is characterized by a summit that lies roughly 3 km above the surrounding terrain with a caldera that drops 500 m below the rim. The diameter of the patera averages ~250 km.

Mapping Tyrrhena's caldera was straightforward. There is only one identifiable unit that continues in an extended channel for 10s of kilometers (Fig. 3h). We included the center and a few km of the lava channel until it changed directions. We initially opted to see if that directional change could have been evidence for a different floor age, but we then excluded that possibility based on crater statistics and combined it with the main caldera and channel.

Resurfacing events are evident from the SFD in Tyrrhena, and we had to exclude some of the channel near the southern walls due to a marked visible deficit of craters. Fitting between 280 and 525 m, we determined a model crater age of $3.41^{+0.08}_{-0.16}$ Ga (Fig. 6h). This agrees well with Werner's (2009) age of 3.29 Ga as well as Williams' et al. (2008) age of $3.2^{+0.3}_{-1.2}$ Ga.

8. Implications for secondary cratering and resurfacing

The issue of secondary craters – relatively small craters that are formed from the ejecta of a primary crater formed by a extra-planetary impactor – was raised as far back as Shoemaker (1965), but it was relegated by the cratering community to a relatively unimportant effect by the 1980s, despite evidence that they may become important on the Moon at diameters smaller than ~1 km (McEwen and Bierhaus, 2006). This has changed in recent years, noticeably in 2005 with separate papers – one discussing mapping of vast, planet-wide fields of secondaries on Europa (Bierhaus et al., 2005), and the other illustrating fields of secondary craters from the Zunil crater on Mars (McEwen et al., 2005). Their work was combined in McEwen and Bierhaus (2006), showing the cratering community that secondary craters were an unresolved and potentially important issue that needs to be taken into account when using craters for age-dating and geologic mapping.

Since then, data returned from the MESSENGER spacecraft has shown that secondary craters on Mercury become important at sizes D < 10 km, a potentially significant issue for mercurian crater age dating (*e.g.*, Strom et al., 2008). In their 2006 paper, McEwen and Bierhaus estimated that secondary craters become statistically important on Mars – where the probability that a given crater is a secondary is ⩾50% – for D < 1 km. As a consequence, our research into dating volcanic calderas where nearly all of our craters are smaller than 1 km provides a test bed for studying the role of secondaries.

One way to determine whether a crater is an "obvious" secondary is that it will be entrained in an elongated clump, where the long axis of the group is oriented radially away from the primary. On Mars, the largest secondary crater is usually only ~2.5–5% the diameter of the primary due to the vastly different impact energy (McEwen and Bierhaus, 2006). They will also usually be shallower than primaries, again due to the lower impact energy. Other classic morphologic features include being generally more elliptical than primary craters due to their lower impact energy, being entrained in other crater ejecta or surrounded by a "herring bone" pattern (*e.g.*, Oberbeck and Morrison, 1974), and/or generally form an annulus of decreasing crater density with increasing distance from the crater. Unfortunately, that is just for "obvious" secondaries. The crux of what McEwen and Bierhaus showed in their respective and joint papers is that there exists a "background field" of secondary craters that cannot be obviously tied to a primary and cannot be morphologically differentiated as a primary versus secondary crater.

Mapping of secondary fields as well as modeling experiments have shown that the SFD of a field of secondary craters roughly follows a $b \approx -4$ power-law slope (*e.g.*, McEwen and Bierhaus, 2006), rising more steeply towards smaller diameters than a standard production function slope of $b \approx -3$. Of primary interest relative to our results, we do not observe this increase in SFD slope in any of the volcanic calderas that we analyzed, save one (see Sections 3.2 and 8.1). The implications for this and possible explanations are discussed below in Section 8.3.

Meanwhile, the two main groups who have worked to establish the crater-frequency age of Mars through isochrons generally do not agree that secondary craters are important (*e.g.*, Hartmann, 2005; Neukum et al., 2006, 2007; Neukum, 2008). For this reason, in an ideal situation where one can assume that the "background field" of secondaries is uniform, then one can still include secondary craters in their SFDs and calculate an accurate age from the established isochrons.

8.1. In-depth analysis of Arsia Mons

When discussing the age of the vast, 10,000 km^2 caldera of Arsia Mons in Section 3.2, we briefly raised the point that Arsia's SFD is the only case where we observed a marked increase in the SFD slope for D < 110 m. Arsia's caldera was also unique in that it was the only case where we observed the "obvious" fields of secondary craters (Fig. 7), but also that there was no obvious nearby primary from which they may have been formed. We mapped the secondary craters we identified in Arsia by their morphology and clustering, and we observed a general northeast–southwest orientation. We used this in an attempt to find a primary, and the closest sizable (~20 km) candidate was ~850 km to the southwest of the volcano and fully 13.5 km lower in elevation than its summit. A potential smaller, ~10 km crater, is located ~450 southwest of the summit and 11.5 km lower in elevation.

After identifying the fields of secondaries, we created separate SFDs showing the secondaries compared with the rest of the craters in the caldera (Fig. 12). For D > 130 m, both SFDs lie along the ~140 Ma isochron. We attribute this to the fields of

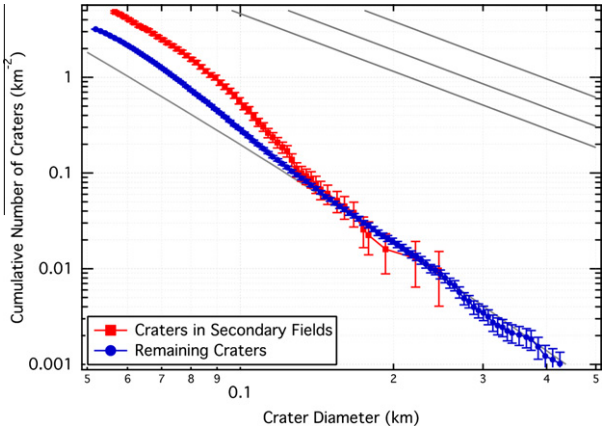

Fig. 12. Size–frequency diagram for Arsia Mons showing the SFD for assumed secondary fields compared with the remaining craters. For $D > 130$ m, both SFDs lie along the ~130 Ma isochron. We attribute this to the fields of secondaries being contaminated by primaries – more detailed modeling would be needed to statistically extract the primaries. At smaller diameters, the secondaries quickly become more numerous and have a steeper slope than the branch of primaries while the slope of the primaries does increase, it does so less significantly, especially at larger diameters, and we can attribute this to an additional population of background secondaries that were not removed along with the "obvious" fields.

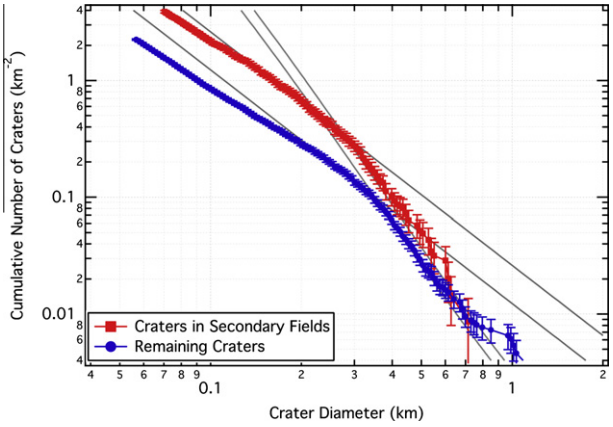

Fig. 13. Size–frequency diagram for Apollinaris Mons showing the SFD for presumed secondary fields contrasted with the SFD for the other craters mapped within calderas 1 and 2. Steep vertical lines are $b \approx -3.78$ isochrons for this diameter range. Shallower lines are $b = -2$ saturation (upper is 1.7% saturation, lower is 0.8% saturation. As shown, the "background" craters have slopes that are shallower than the isochrons for $D > 500$ m, matches the isochron for $350 < D < 500$ m, matches saturation for $225 < D < 350$ m, and then falls below saturation at smaller diameters. The "secondary" region craters have a statistically insignificant steeper slope for $550 < D < 725$ m, generally match the slopes of the background craters, and follow empirical saturation over a much larger diameter range, through ~125 m.

secondaries being contaminated by primaries – more detailed modeling would be needed to statistically extract the primaries. At smaller diameters, the secondaries quickly become more numerous and have a steeper slope than the branch of primaries, as theory would predict (*e.g.*, McEwen and Bierhaus, 2006). While the slope of the primaries does increase, it does so less significantly, especially at larger diameters, and we can attribute this to an additional population of background secondaries that were not removed along with the "obvious" fields.

These results have two important implications. First, the background field of secondary craters on Mars is likely to exist, in contrast with Neukum (2008) and Werner et al. (2009), and they can exist with no obvious primary crater anywhere near them. The second implication is that, while we observe the SFD enhancement of secondaries, it occurs at a diameter 10% that estimated by McEwen and Bierhaus (2006). While one example does not make a case for the ~100 m diameter being the *maximum* diameter at which secondaries become important (that we observed), it at least raises the issue that there may not be a uniform size dependence across the planet, further complicating the role of secondaries.

8.2. In-depth analysis of Apollinaris Mons

We discussed the opposite case to Arsia Mons in Section 6, Apollinaris Mons. While Arsia's SFD showed an increase of slope attributable to secondaries, Apollinaris did not. Where there were morphologically obvious fields of secondaries in Arsia's caldera, no such fields exist in Apollinaris'. And while there was no obvious nearby primary to form the fields in Arsia, there were three, quite obvious, large primaries that formed nearby secondaries in an annulus about the primary (Fig. 11).

In an attempt to examine the SFD slope of the secondaries, we isolated the regions of enhanced craters within calderas 1 and 2. We then created SFDs for these and compared them with the rest of the craters in the two calderas, shown in Fig. 13. The results are inconclusive. The "background" craters have slopes that are shallower than the isochrons for $D > 500$ m, match the isochron for $350 < D < 500$ m, match saturation for $225 < D < 350$ m, and then fall below saturation at smaller diameters. The "secondary" regions' craters have a statistically insignificant steeper slope for $550 < D < 725$ m, generally match the slopes of the background craters, and follow empirical saturation over a much larger diameter range, through ~125 m. We cannot say for certain from analysis of the SFDs that these regions are dominated by secondaries, though we do maintain this is the likely case based upon the locations of enhanced crater density.

8.3. Possible model interpretations and explanations

While McEwen and Bierhaus (2006) estimated that secondaries become important on Mars for $D < 1$ km, it should be apparent from our SFDs that this is at least not the case for the caldera regions that we studied (totals 0.0356% of the global surface area), although the only methods we used to search for secondary craters was visual inspection of the CTX data and hence we were not exhaustive of all methods. One possible way to explain this while still maintaining the $D < 1$ km size as the transition diameter is to suggest that the rate of resurfacing in all these calderas is greater than the production rate of secondary craters. For this to be the case, we can estimate what the resurfacing rate must be as we show in the following:

A 1 km primary crater has a nominal depth of 100 m (10% the diameter) (Melosh, 1989). Secondary craters are shallower, generally by 50%, so a 1 km secondary crater is ideally 50 m deep (Melosh, 1989). From Hartmann and Neukum (2001), the average formation rate of a 1 km primary crater between 1 and 3 Ga was 10^{-3} km^{-2}. If we assume a $b = -3$ power-law slope for the production of craters at Mars (Hartmann, 2005), and we require a minimum of a 20-km primary crater to form a 1 km secondary (McEwen and Bierhaus, 2006), then we would expect a $D = 1$ km secondary crater to form on Mars roughly once every 5 Myr. To then erase that crater would require a minimum erosion rate >10 nm/year.

This is a fairly rapid rate compared with previous works: From mapping Zunil crater, Preblich et al. (2007) estimated a rate $\geqslant$80 nm/year. Golombek et al. (2007) estimated a rate of 1.3 nm/year in the Late Amazonian from the Mars Exploration Rover landing sites, though noted average erosion rates of 0.03 nm/year in the Gusev Crater floor, 0.02 nm/year at the Mars Pathfinder site, and

1 nm/year at the Viking Lander 1 site. However, they noted higher erosion rates of 1–10 nm/year since the Hesperian (~3.5 Ga) in Meridiani Planum. This is comparable to rates determined by Hartmann (2003) of 0.05–2 nm/year for the rate of crater infilling, perhaps the best direct comparison to our suggested rate for this model. In sum, we think it is unlikely that normal erosive processes can account for the lack of a secondary crater branch on our SFDs, considering that not only do not we see the increase due to secondaries (except at Arsia), but we see a more rapid decrease in the SFDs at smaller diameters than expected at most locations.

An alternative model to save the 1 km transition diameter is to argue that volcanic material on the surface undergoes alteration over time that changes the production of secondaries (*e.g.*, as proposed by Hartmann and Barlow (2006)). Since Apollinaris Mons has the oldest surface age of the volcanoes we dated, one may expect that its near-surface material may be well gardened and most similar to the bulk crust of Mars, therefore secondaries would lie closest to primaries on it; one could also argue at least for $D < 250$ m that it is empirically saturated already and the SFD will not reflect additional secondaries (Figs. 6f and 13). Conversely, with the Tharsis region having a young surface, we could expect the issues with volcanic terrain producing secondaries to be best reflected there. This is somewhat buoyed by the lack of SFD enhancement attributable to secondaries on the young (1.42 ± 0.30 Ga) Ulysses Patera. However, this model is not supported by the lack of secondaries around the large crater in the middle of caldera 1 in Hadriaca Patera: aged at 3.1 ± 0.1 Ga, this is only ~800 Myr younger than the oldest Apollinaris Mons caldera, and while matching 8‰ geometric saturation, a value this low strains believability as an explanation. More work would need to be done with a Zunil-type crater on volcanic terrain (*e.g.*, somewhere on Tharsis) to determine if this may be a valid explanation.

Instead, we propose a more likely explanation that – at least in our regions of study – secondary craters do not become statistically important on Mars for $D \leqslant 1$ km but rather at sizes 1–2 orders of magnitude smaller. However, secondaries are still important to consider in crater counting statistics – as evidenced by their presence in Apollinaris but not reflected in its SFD – and our work supports the models that suggest there is a broad background secondary field across Mars, though we question the diameter previously proposed at which it becomes statistically important (*i.e.*, McEwen and Bierhaus, 2006). We think that more studies over a broader area are needed to help answer this ongoing question.

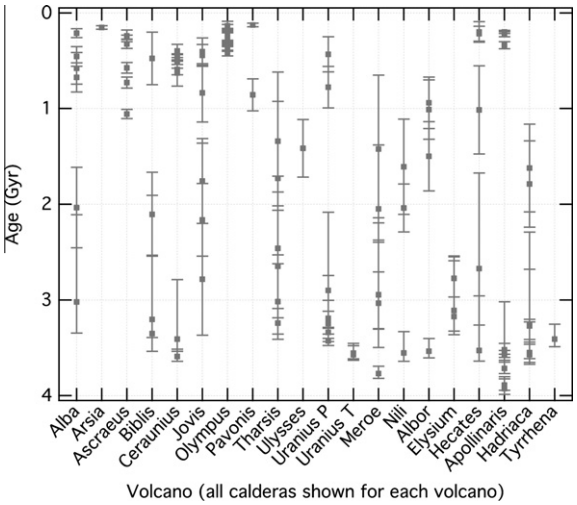

Fig. 14. Timeline illustrating the ages discussed in the text and Table 2 for every volcano in this study. Split ages for a single caldera are included in this figure, even though several are likely due to resurfacing processes (*e.g.*, Ceraunius Tholus for calderas 3 and 4).

9. Implications for the history of volcanism on Mars

A timeline with all caldera ages discussed in Sections 3–7 is shown in Fig. 14, and we illustrate these over the main epochs of geologic history on Mars in Fig. 15. We also provide a movie of this sequence in online supplemental material. Before our summary analysis, we reiterate two main constraints on our study. First, we dated the caldera surfaces, therefore our conclusions are limited to the last episodes of volcanism from the summit of each volcano. For example, we fully expect that Arsia Mons is an old volcano, having been built up over several billion years (*e.g.*, Hodges and Moore, 1994 and references therein; Anderson et al., 2001), but its single caldera has a modeled crater age of 130 Ma and so that is the age we report. This also ignores several of the younger vents that surround it. Second, approximately 20% of the calderas we dated were given split ages. Often, we attributed this to resurfacing events, such as Ceraunius Tholus' calderas 3 and 4 (Section 3.5). In a few cases, such as Olympus Mons, the older age is at a smaller diameter and this is difficult to explain. However, because we cannot state conclusively a non-volcanic reason for these counterintuitive observations, we have displayed both ages in all cases in Fig. 14. There have been many previous authors who have derived crater ages in the past (numerous references throughout this paper), and the purpose of our results is to help refine these ages and last episodes of volcanism. Finally, in the discussion below, Mars' epochs are based on the times given in Hartmann and Neukum (2001).

Apollinaris Mons shows the oldest caldera ages, dating back to 3.9 Ga. It was also the first volcano to die out, its activity ending around the start of the Hesperian (if we attribute the lone split ages of 200 and 220 Ma for calderas 3 and 6 to non-volcanic resurfacing events). This is in contrast with the nearby Elysium region, where Elysium Mons ceased activity approximately 3 Ga, but the two nearby tholi (Hecates and Albor) show ages that date from that period to fairly recent. This adds to the case that Apollinaris Mons likely had a different magma source than Elysium, and it should be considered completely separate from that complex.

Moving to the circum-Hellas highlands volcanoes, Tyrrhena Patera shows a complex erosional history, but its last volcanism died out squarely within the Hesperian epoch. This contrasts with the Hadriaca volcano which shows crater ages that span over 2 Gyr of martian history, ending around 1.6 Ga. This is also approximately when the Syrtis Major volcanoes ceased large-scale activity. Meroe and Nili Paterae show ages almost as old as Apollinaris, but then sporadic activity though ~1.4 Ga, with the split age of 230 Ma in Meroe's caldera 5 likely due to non-volcanic resurfacing events.

The vast Tharsis region, fully 60% of the volcanoes we studied, shows no obvious trends in ages in terms of latitude/longitude distributions. We note that generally the smallest volcanoes – Biblis, Ceraunius, Tharsis, and Uranius Tholi along with Uranius Mons – show the oldest caldera ages, while it is generally the largest volcanoes – Arsia, Ascraeus, Olympus, and Pavonis Montes – that show the youngest (in agreement with previous works, such as Hodges and Moore (1994) and Werner (2009)). The most notable exception is the vast Alba Mons that shows caldera ages ranging between 3.0 Ga and ~300 Ma. This adds to the uniqueness of Alba Mons that has been recognized before as a transitional volcano between explosive and effusive volcanism (*e.g.*, Raitala, 1989; Ivanov and Head, 2006).

Broadly from our analysis, we can conclude that Mars has had active large-scale volcanism at least until ~100–150 myr ago (constrained by the Arsia, Olympus, and Pavonis Montes). Every volcano we studied was active through the Hesperian epoch, while all except for Tyrrhena Patera and Apollinaris Mons were active through at least the Early Amazonian. Only the Syrtis Major calderas and Apollinaris Mons show ages that date to the Noachian time,

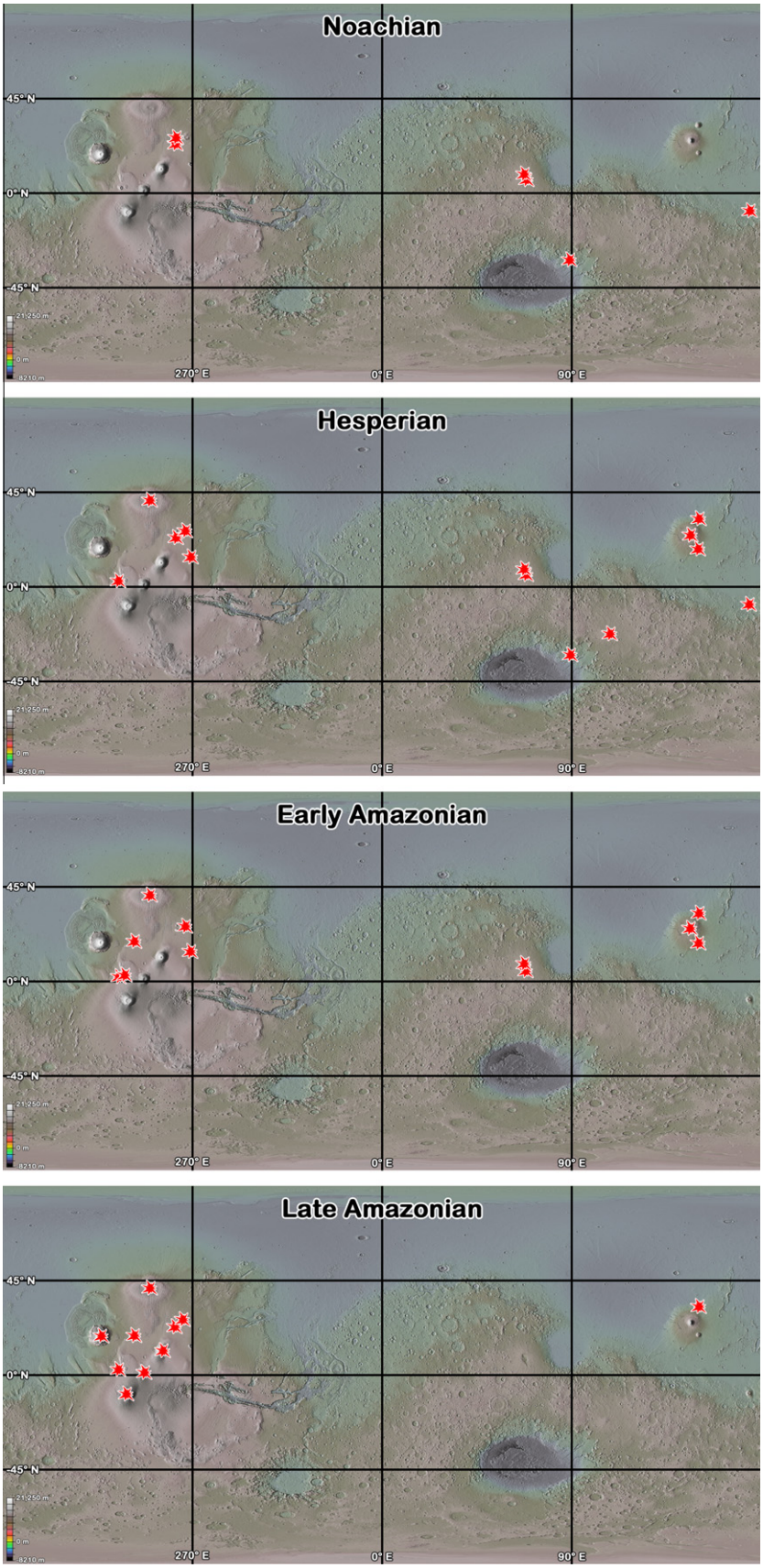

Fig. 15. Following the ages in Fig. 13, we illustrate here roughly the ages of the calderas during the Noachian, Hesperian, Early Amazonian, and Late Amazonian. We also provide a movie to illustrate this sequence in online supplemental material.

indicating that volcanism likely died out rapidly in those areas in early martian history. This is consistent with the evidence for widespread volcanic flooding during the Hesperian that has been identified by other researchers (*e.g.*, Greeley and Spudis, 1981; Head et al., 2002).

We do observe a trend in the ages of the three Tharsis Montes, which are Ascraeus, Pavonis, and Arsia, from north to south (similar to previous findings, *e.g.* Hodges and Moore, 1994 and references therein). Ascraeus' calderas show six distinct ages, ranging in time from approximately 1.1 Ga to 250 Ma. Pavonis' calderas date to 850 Ma and 130 Ma, while Arsia's single caldera dates to ~140 Ma. In short, they all die out roughly within ~100 Myr of each other, while their oldest calderas are successively older northward. This could be simple random chance since there is a sample size of three. Or, a possible explanation is that a branching plume fed all three montes and successively died out southward. This runs contrary to a model proposed by Bleacher et al. (2007). They suggest an original mantle upwelling fed Arsia, branched and spread to Pavonis, and continued to migrate northward with the two branches eventually settling under Pavonis and Ascraeus. We suggest effectively the opposite based on our derived ages; clearly, more work needs to be done in this area and one needs to consider both the crater ages of the surface as well as surrounding geomorphologic properties.

Finally, we can relate our results to a broad transition from explosive to effusive volcanism, generally attributed to a decreasing near-surface water table (*e.g.*, Mouginis-Mark et al., 1988). Explosive/pyroclastic eruption styles on Earth in silica-poor magmas generally occur when there is a high water content. On Mars, this can be generalized to volatiles in the magma. As the magma rises, the volatiles are under less pressure and can explosively separate from the liquid rock. In contrast, effusive flows lack volatiles and correspond more towards a steadier, less viscous morphology. This will generally produce two identifiable features, the first being that effusive flows will have more competent lavas that have flow-like morphologies emanating from the source, and second is there will generally be a better-defined caldera rim for the effusive type (Wilson and Head, 1994). A large caveat to this analysis stems from our ability to only assess eruption style based on the calderas we mapped. In-depth morphological studies of the entirety of each volcano and related deposits is beyond the scope of this work. For example, below, we classify Hecates Tholus as primarily effusive in style even though numerous previous researchers have noted potential pyroclastic deposits (*e.g.*, Mouginis-Mark et al., 1988). Another example is Olympus Mons, which we also classify as effusive from its calderas, though previous theoretical and observational work has shown it may have a significant component of pyroclastics (*e.g.*, Head and Wilson, 1998a,b; Wilson et al., 1998).

From these morphologic predictions and with these caveats in mind, we can classify Apollinaris Mons, Elysium Mons, Syrtis Major, Uranius Tholus, the circum-Hellas vents Hadriaca and Tyrrhena Paterae, and some of Alba Mons as primarily explosive. The majority of the Tharsis volcanoes and Elysium tholi show more of an effusive morphology. From Fig. 14, we can roughly place that transition at ~3.2–3.5 Ga, around the time of the Hesperian epoch and Hesperian/Amazonian transition. It likely happened at different times for different geographic locations, and more detailed morphologic studies would be needed to characterize this with greater accuracy (*e.g.*, the meticulous study of Alba Mons provided in Ivanov and Head (2006)).

10. Discussion and conclusions

With the notable exception of the systematic study by Werner (2009), all previous work in dating Mars' volcanoes was done by different researchers at different times using disparate imagery data and various isochron chronologies. This creates unknown systematic and non-systematic uncertainties throughout the literature and limits the utility of combining the results to piece together as accurate a timeline of volcanism on the planet as is possible today. The work presented here varies from Werner (2009) by using a different, higher-resolution imagery set (CTX from Mars Reconnaissance Orbiter as opposed to HRSC from Mars Express), and it focuses on dating each individual caldera or terrace within the volcanic caldera complex for 20 major martian volcanoes. In contrast, Werner (2009) bulk-dated many of the calderas and ignored about half of them in favor of age dating the volcanic edifice and/or surrounding flows. As a consequence, our present study represents the highest-resolution imagery-based crater-model-age-based chronology for the last episodes of volcanism from all major martian volcanoes (save Amphitrites, Malea, Peneus, and Pityusa Paterae).

In the text, we have compared our results to Neukum et al. (2004), Williams et al. (2007, 2008), and Werner (2009) where comparisons could be made. Overall, we are in good agreement with Williams et al. (2007, 2008), and our ages are generally older than but still mostly comparable with Neukum et al. (2004) once statistical uncertainties are taken into account. When comparing with Werner (2009), we make the interesting observation that the published results are identical with Neukum et al. (2004) for the volcanoes they both did – in general, younger than ours – but otherwise the rest are split between older and younger. We are within each others' uncertainties more than 50% of the time.

A probable explanation for why our ages are generally older than Neukum et al. (2004) is that we are using higher resolution data and hence likely are complete to smaller diameters. This is supported via direct comparisons between our SFDs and those published in both Neukum et al. (2004) and Werner (2009). From visual inspection of figures from these papers, they generally appear complete to around the 100–200 m level, while our completeness varies between ~50 and 75 m. We also note that the often-used $N(1)$, $N(5)$, or similar type of crater age based on a single diameter size is insufficient to obtain an accurate crater model age unless the SFDs are well behaved; as we show in Figs. 5 and 6, this is rarely the case. It is difficult to know over what range these two sets of authors fit isochrons because that data are not published, and in the earlier paper the figures are not high enough resolution for a meaningful comparison.

We have used our CTX-based crater counts to construct a timeline for the last volcanic activity from each major volcano's calderas (Figs. 14 and 15, and online supplemental movie). We confirm that Mars has had almost continuous active volcanism throughout its geologic history, with major volcanism ceasing only ~100–150 myr ago, 98% through the planet's history. We note a change from explosive to effusive styles of eruption transitioning at different times across the planet, but generally the transition was made around the Hesperian–Amazonian boundary. We also have shown evidence that volcanism has "shut off" in different locations at different times as Mars' interior has cooled. This started with Apollinaris Mons, continued through the rest of the highlands and Syrtis Major, and ended with the Elysium tholi and the largest of the Tharsis volcanoes.

Besides deriving surface ages to add to the broader picture of Mars' volcanic history, we have used the craters to study implications for the role of secondary craters across the planet. We did not find evidence for a general "background field" of secondaries that becomes statistically important – as determined by an increase in slope of SFDs – for diameters $D \leqslant 1$ km, contrary to expectations from McEwen and Bierhaus (2006), though this could be due to the relatively isolated regions we examined. We did find evidence that secondaries can occur close to their primaries (Apollinaris Mons)

but can be indistinguishable from primaries based on morphology alone; we also found they may not occur next to larger primaries (such as in Hadriaca and Ulysses Paterae). Conversely, we also confirmed previous results that secondaries can occur very far from a primary crater yet still maintain the classic morphology associated with them (Arsia Mons). These conflicting cases do not have an obvious simple resolution, leaving secondary crater studies still a necessary area of future research.

In an attempt to explain the paucity of secondary craters below 1 km, we used a simple model of crater flux and scaling laws to determine the necessary erosion rate to just maintain a standard SFD, not even factoring in that we often found SFDs showing evidence of additional heavy erosion. We found an unreasonably rapid requisite erosion rate approximately 10× higher than previous estimates would be necessary to account for this. We also verified using higher-resolution imagery for limited locations that we are statistically complete to the crater sizes that we claim, despite the significant decrease in the expected number of craters across several calderas.

Finally, if we assume there are no other young volcanic terrains on Mars that are not associated with a major volcano, ignore the factor of ~2 uncertainty in current isochrons, and take our model crater ages as the actual ages for the volcanoes, we can speculate that most of the martian meteorites, dating to only a ~few 100 Myr, likely came from the younger flows of the Tharsis Montes. This is in agreement with some other researchers' speculations based on crater ages (*e.g.*, Hartmann, 2005), but it disagrees with others based on spectra (*e.g.*, Hamilton et al., 2003), modeling of inferred crystallization versus modification ages (Bouvier et al., 2005), and some interpretations of geologic and petrologic data (McSween, 2002).

Overall, Mars continues to yield more information with higher-resolution imagery, and much can be gleaned from crater studies especially when geologic and geomorphologic context is used in concert. We believe that studies of volcanic calderas with even higher resolution data would not be useful due to the significant resurfacing we observed at the decameter scale in most cases, and that future work should be focused on continuing to map the flanks and studying the characteristics and implications of secondary craters on volcanic terrain.

Acknowledgments

This paper benefited from useful discussions with E.B. Bierhaus and two anonymous reviewers. S.J. Robbins was supported through NASA NESSF Award NNX07AU85H. G. Di Achille was supported through NASA Grant Award NNX07AU41G. B.M. Hynek was supported through NASA Awards NNX07AU41G and NNX06AE08G.

Appendix A. Supplementary material

Supplementary data associated with this article can be found, in the online version, at doi:10.1016/j.icarus.2010.11.012.

References

Anderson, R.C., Dohm, J.M., Golombek, M.P., Haldemann, A.F.C., Franklin, B.J., Tanaka, K.L., Lias, J., Peer, B., 2001. Primary centers and secondary concentrations of tectonic activity through time in the western hemisphere of Mars. J. Geophys. Res. 106 (E9), 20563–20585.

Andrews-Hanna, J.C., Zuber, M.T., Banerdt, W.B., 2008. The Borealis Basin and the origin of the martian crustal dichotomy. Nature 453, 1212–1215. doi:10.1038/nature07011.

Arvidson, R. et al., 1979. Standard techniques for presentation and analysis of crater size–frequency data. Icarus 37, 467–474.

Barlow, N.G., 1988. Crater size–frequency distributions and a revised martian relative chronology. Icarus 75, 285–305. doi:10.1016/0019-1035(88)90006-1.

Berman, D.C., Hartmann, W.K., 2002. Recent fluvial, volcanic, and tectonic activity on the Cerberus Plains of Mars. Icarus 159, 1–17. doi:10.1006/icar.2002.6920.

Bierhaus, E.B., Chapman, C.R., Merline, W.J., 2005. Secondary craters on Europa and implications for cratered surfaces. Nat. Lett. 437, 1125–1127. doi:10.1038/nature04069.

Blasius, K.R., 1976. The record of impact cratering on the great volcanic shields of the Tharsis region of Mars. Icarus 29, 343–361. doi:10.1016/0019-1035(76)90138-X.

Bleacher, J.E., Greeley, R., Williams, D.A., Cave, S.R., Neukum, G., 2007. Trends in the effusive style at the Tharsis Montes, Mars, and implications for the development of the Tharsis Province. J. Geophys. Res. 112, 1–15. E09005. doi:10.1029/2006JE002873.

Bouvier, A., Blichert-Toft, J., Vervoort, J.D., Albarède, F., 2005. The age of SNC meteorites and the antiquity of the martian surface. Earth Planet. Sci. Lett. 240, 221–233. doi:10.1016/j.epsl.2005.09.007.

Cattermole, P., Reid, C., 1984. The summit calderas of Alba Patera, Mars. Lunar Planet. Sci. XV. 15, 142–143.

Christensen, P.R. et al., 2004. The Thermal Emission Imaging System (THEMIS) for the Mars 2001 Odyssey Mission. Space Sci. Rev. 110 (1), 85–130. doi:10.1023/B:SPAC.0000021008.16305.94.

Di Achille, G., Hynek, B.M., 2010. Deltas and valley networks on Mars: Implications for a global hydrosphere. In: Cabrol, Grin (Eds.), Lakes on Mars. Elsevier Publishing. ISBN/9780444528544 (Chapter 8).

Fassett, C.I., Head III, J.W., 2007. Valley formation on martian volcanoes in the Hesperian: Evidence for melting of summit snowpack, caldera lake formation, drainage and erosion on Ceraunius Tholus. Icarus 189, 118–135. doi:10.1016/j.icarus.2006.12.021.

Golombek, M.P. et al., 2007. Climate change on Mars from erosion rates at the Mars Exploration Rover landing sites. In: 7th Int. Conf. on Mars 7. Abstract #3034.

Grant, J.A. et al., 2004. Surficial deposits at Gusev Crater along Spirit Rover traverses. Science 305, 807–810. doi:10.1126/science.1099849.

Greeley, R., Spudis, P.D., 1981. Volcanism on Mars. Rev. Geophys. 19, 13–41.

Hamilton, V.E., Christensen, P.R., McSween Jr., H.Y., Bandfield, J.L., 2003. Searching for the source regions of martian meteorites using MGS TES: Integrating martian meteorites into the global distribution of igneous materials on Mars. Meteorit. Planet. Sci. 38, 871–885.

Hare, T.M., Skinner, J.A., Tanaka, K.L., Fortezzo, C.M., Bleamaster, L.F., Sucharski, R.M., 2009. GIS-based planetary geologic maps: Recommendations for improved preparation, review, and publication. Lunar Planet. Sci. XL. Abstract #2538.

Hartmann, W.K., 2003. Measurement of martian erosion/obliteration rates from crater populations. AGU, p. 7354.

Hartmann, W.K., 2005. Martian cratering 8: Isochron refinement and the chronology of Mars. Icarus 174, 294–320. doi:10.1016/j.icarus.2004.11.023.

Hartmann, W.K., Barlow, N., 2006. Nature of the martian uplands: Effect on the martian meteorite age distribution and secondary cratering. Meteorit. Planet. Sci. 41, 1453–1467.

Hartmann, W.K., Neukum, G., 2001. Cratering chronology and the evolution of Mars. Space Sci. Rev. 96, 165–194.

Hauber, E., Bleacher, J., Gwinner, K., Williams, D., Greeley, R., 2009. The topography and morphology of low shields and associated landforms of plains volcanism in the Tharsis region of Mars. J. Volcanol. Geotherm. Res. 185, 69–95. doi:10.1016/j.volgeores.2009.04.015.

Hauber, E., Brož, P., Jagert, F., 2010. Plains volcanism on Mars: Ages and rheology of lavas. Lunar Planet. Sci. XLI. Abstract #1298.

Head, J.W., Wilson, L., 1998a. Tharsis Montes as composite volcanoes?: 1. The role of explosive volcanism in edifice construction and implications for the volatile contents of edifice-forming magmas. Lunar Planet. Sci. XXIX. Abstract #1127.

Head, J.W., Wilson, L., 1998b. Tharsis Montes as composite volcanoes?: 3. Lines of evidence for explosive volcanism in edifice construction. Lunar Planet. Sci. XXIX. Abstract #1124.

Head, J.W., Kreslavsky, M.A., Pratt, S., 2002. Northern lowlands of Mars: Evidence for widespread volcanic flooding and tectonic deformation in the Hesperian Period. J. Geophys. Res. – Planets 107, 5003. doi:10.1029/2000JE001445.

Hodges, C.A., Moore, J.J., 1994. Atlas of Volcanic Landforms on Mars. US GPO, Washington.

Ivanov, B.A., 2001. Mars/Moon cratering rate ratio estimates. Chronol. Evol. Mars 96, 87–104.

Ivanov, M.A., Head, J.W., 2006. Alba Patera, Mars: Topography, structure, and evolution of a unique late Hesperian–early Amazonian shield volcano. J. Geophys. Res. 111 (E09003), 1–31. doi:10.1029/2005JE002469.

Lang, N.P., McSween, H.Y., Tornabene, L.L., Hardgrove, C.J., Christensen, P.R., 2010. Re-examining the relationship between Apollinaris Patera and the basalts of the Gusev Crater plains, Mars. J. Geophys. Res. – Planets 115, E14. doi:10.1029/2009JE003397.

Lapen, T.J., Righter, M., Brandon, A.D., Debaille, V., Beard, B.L., Shafer, J.T., Peslier, A.H., 2010. A younger age for ALH84001 and its geochemical link to Shergottite sources on Mars. Science 328, 347–351. doi:10.1126/science.1185395.

Malin, M.C. et al., 2007. Context camera investigation on board the Mars Reconnaissance Orbiter. J. Geophys. Res. 112, E5. doi:10.1029/2006JE002808.

McEwen, A.S., Bierhaus, E.B., 2006. The importance of secondary cratering to age constraints on planetary surfaces. Annu. Rev. Earth Planet. Sci. 34, 535–567. doi:10.1146/annurev.earth.34.031405.125018.

McEwen, A.S., Preblich, B.S., Turtle, E.P., Artemieva, N.A., Golombek, M.P., Hurst, M., Kirk, R.L., Burr, D.M., Christensen, P.R., 2005. The rayed crater Zunil and interpretations of small impact craters on Mars. Icarus 176, 351–381. doi:10.1016/j.icarus.2005.02.009.

McEwen, A.S. et al., 2007. Mars Reconnaissance Orbiter's High Resolution Imaging Science Experiment (HiRISE). J. Geophys. Res. 112, E5. doi:10.1029/2005JE002605.
McSween Jr., H.Y., 2002. The rocks of Mars, from far and near. Meteorit. Planet. Sci. 37, 7–25.
Melosh, H.J., 1989. Impact Cratering: A Geologic Process. Oxford University Press, New York.
Morris, R.V. et al., 2008. Iron mineralogy and aqueous alteration from Husband Hill through Home Plate at Gusev Crater, Mars: Results from the Mössbauer instrument on the Spirit Mars Exploration Rover. J. Geophys. Res. – Planets 113 (E12). doi:10.1029/2008JE003201.
Mouginis-Mark, P.J., Wilson, L., Zibelman, J.R., 1988. Polygenic eruptions on Alba Patera, Mars. Bull. Volcanol. 50, 361–379. doi:10.1007/BF01050636.
Neukum, G., 2008. The lunar and martian cratering records and chronologies. Lunar Planet. Sci. XXXIX. Abstract #2509.
Neukum, G., Hiller, K., 1981. Martian ages. J. Geophys. Res. 86, 3097–3121. doi:10.1029/JB086iB04p03097.
Neukum, G., Hiller, K., Henkel, J., Bodechtel, J., 1979. Surface ages of martian shield volcanoes and channels. Lunar Planet. Sci. X, 907–909.
Neukum, G., Ivanov, B.A., Hartmann, W.K., 2001. Cratering records in the inner Solar System in relation to the lunar reference system. Chronol. Evol. Mars 96, 55–86.
Neukum, G. et al., 2004. Recent and episodic volcanic and glacial activity on Mars revealed by the High Resolution Stereo Camera. Nature 432, 971–979.
Neukum, G., Werner, S.C., Ivanov, B.A., 2006. The Characteristics of the Impact Crater Production Size–Frequency Distributions on the Solar System Planetary Bodies, their Relationships to Asteroidal and Cometary Impacts, and the Question of Secondary-Cratering Contributions. Planetary Chronology Workshop. Abstract #6005.
Neukum, G. et al., 2007. Episodicity in the geological evolution of Mars: Resurfacing events and ages from cratering analysis of image data and correlation with radiometric ages of martian meteorites. In: 7th Int. Conf. Mars 7. Abstract #3015.
Nimmo, F., Tanaka, K., 2005. Early crustal evolution of Mars. Annu. Rev. Earth Planet. Sci. 33, 133–161. doi:10.1146/annurev.earth.33.092203.122637.
Nyquist, L.E., Bogard, D.D., Shih, C.-Y., Greshake, A., Stöffler, D., Eugster, O., 2001. Ages and geologic histories of the martian meteorites. Chronol. Evol. Mars 96, 105–164.
Oberbeck, V.R., Morrison, R.H., 1974. Laboratory simulation of the herringbone pattern associated with lunar secondary crater chains. Moon 9, 415–455. doi:10.1007/BF00562581.
Pasckert, J.H., Hiesinger, H., Reiss, D., 2010. Rheology and age of lava flows on Elysium Mons, Mars. Lunar Planet. Sci. XLI. Abstract #1903.
Peterson, J.E., 1978. Volcanism in the Noachis–Hellas region of Mars, 2. Proc. Lunar. Sci. Conf. 9, 3411–3432.
Plescia, J.B., 1994. Geology of the small Tharsis volcanoes: Jovis Tholus, Ulysses Patera, Biblis Patera, Mars. Icarus 111, 246–269.
Plescia, J.B., Saunders, R.S., 1979. The chronology of the martian volcanoes. Proc. Lunar. Sci. Conf. 10, 2841–2859.
Preblich, B.S., McEwen, A.S., Studer, D.M., 2007. Mapping rays and secondary craters from the martian crater Zunil. J. Geophys. Res. 112, 1–18. E05006. doi:10.1029/2006JE002817.
Putzig, N.E., Mellon, M.T., 2007. Apparent thermal inertia and the surface heterogeneity of Mars. Icarus 191, 68–94. doi:10.1016/j.icarus.2007.05.013.
Rafkin, S.C.R., Michaels, T.I., 2003. Meteorological predictions for 2003 Mars Exploration Rover high-priority landing sites. J. Geophys. Res. 108 (E12), 1–23. doi:10.1029/2002JE002027.
Raitala, J., 1989. Development of the Alba Patera volcano on Mars. Adv. Space Res. 9 (6), (6)143–(6)146.
Roberts, G.P., Crawford, I.A., Peacock, D., Vetterlein, J., Parfitt, E., Bishop, L., 2007. Possible evidence for on-going volcanism on Mars as suggested by thin, elliptical sheets of low-albedo particulate material around pits and fissures close to Cerberus Fossae. Earth Moon Planets 101, 1–16. doi:10.1007/s11038-007-9140-.
Shoemaker, E.M., 1962. Interpretation of lunar craters. In: Kopal, Z. (Ed.), Physics and Astronomy of the Moon. Academic, New York, pp. 283–359.
Shoemaker, E.M., 1965. Preliminary analysis of the fine structure of the lunar surface in Mare cognitum. In: Heiss, W.N., Menzel, D.R., O'Keefe, J.A. (Eds.), The Nature of the Lunar Surface. Johns Hopkins Press, Baltimore, pp. 23–77 (JPL Tech. Report no. 32-700).
Smith, D.E. et al., 2001. Mars Orbiter Laser Altimeter: Experiment summary after the first year of global mapping on Mars. J. Geophys. Res. 106, 23689–23722. doi:10.1029/2000JE001364.
Solomon, S.C. et al., 2005. New perspectives on ancient Mars. Science 307, 1214–1220. doi:10.1126/science.1101812.
Strom, R.G., Chapman, C.R., Merline, W.J., Solomon, S.C., Head, J.W., 2008. Mercury cratering record viewed from MESSENGER's first flyby. Science 321, 79–81. doi:10.1126/science.1159317.
Tanaka, K.L., 1982. A new time-saving crater-count technique, with application to narrow features. In: Holt, H.E. (Ed.), Planetary Geology and Geophysics Program Report, NASA Technical Memo., NASA TM-85127, pp. 123–125.
Tanaka, K.L., Isabell, N.K., Scott, D.H., Greeley, R., Guest, J.E., 1988. The resurfacing history of Mars: A synthesis of digitized, Viking-based geology. Proc. Lunar. Sci. Conf. 18, 665–678.
Tanaka, K.L., Hare, T.M., Skinner, J.A., 2005. Geologic Map of the Northern Plains of Mars. US Geol. Surv. Misc. Invest. Ser. Map, I-2888.
Tanaka, K.L., Skinner, J.A., Crumpler, L.S., Dohm, J.M., 2009. Assessment of planetary geomorphologic mapping techniques for Mars using terrestrial analogs: The SP Mountain area of the San Francisco Volcanic Field, Arizona. Planet. Space Sci. 57, 510–532. doi:10.1016/j.pss.2008.06.012.
Werner, S.C., 2009. The global martian volcanic evolutionary history. Icarus 201, 44–68. doi:10.1016/j.icarus.2008.12.019.
Werner, S.C., Ivanov, B.A., Neukum, G., 2009. Theoretical analysis of secondary cratering on Mars and an image-based study on the Cerberus Plains. Icarus 200, 406–417. doi:10.1016/j.icarus.2008.10.011.
Williams, D.A., Greeley, R., Zuschneid, W., Werner, S.C., Neukum, G., Crown, D.A., Gregg, T.K.P., Gwinner, K., Raitala, J., 2007. Hadriaca Patera: Insights into its volcanic history from Mars Express High Resolution Stereo Camera. J. Geophys. Res. 122, 1–18. E10004. doi:10.1029/2007JE002924.
Williams, D.A., Greeley, R., Werner, S.C., Michael, G., Crown, D.A., Neukum, G., Raitala, J., 2008. Tyrrhena Patera: Geologic history derived from Mars Express High Resolution Stereo Camera. J. Geophys. Res. 113, 1–14. E11005. doi:10.1029/2008JE003104.
Williams, D.A. et al., 2009. The Circum-Hellas Volcanic Province, Mars: Overview. Planet. Space Sci. 57, 895–916. doi:10.1016/j.pss.2008.08.010.
Wilson, L., Head III, J.W., 1994. Mars: Review and analysis of volcanic eruption theory and relationships to observed landforms. Rev. Geophys. 32, 221–263.
Wilson, L., Head, J.W., Mitchell, K.L., 1998. Tharsis Montes as composite volcanoes?: 2. Lines of evidence for explosive volcanism in far-field deposits. Lunar Planet. Sci. XXIX. Abstract #1125.
Zhong, S., 2009. Migration of Tharsis volcanism on Mars caused by differential rotation of the lithosphere. Nat. Geosci. 2, 19–23. doi:10.1038/ngeo392.